N2O production and consumption from stable isotopic and concentration data in the Peruvian coastal upwelling system

Annie Bourbonnais, Robert T. Letscher, Hermann W. Bange, Vincent Echevin, Jennifer Larkum, Joachim Mohn, Naohiro Yoshida, Mark A. Altabet

AGU PUBLICATIONS

Global Biogeochemical Cycles

RESEARCH ARTICLE
10.1002/2016GB005567

Key Points:
- High N_2O concentrations were observed in coastal waters off Peru
- Incomplete denitrifier-denitrification was an important N_2O production pathway
- N_2O production occurred at high extent of N loss in the shallow ODZ

Supporting Information:
- Supporting Information S1
- Supporting Information S2

Correspondence to:
A. Bourbonnais,
abourbonnais@whoi.edu

Citation:
Bourbonnais, A., R. T. Letscher, H. W. Bange, V. Échevin, J. Larkum, J. Mohn, N. Yoshida, and M. A. Altabet (2017), N_2O production and consumption from stable isotopic and concentration data in the Peruvian coastal upwelling system, *Global Biogeochem. Cycles*, *31*, 678–698, doi:10.1002/2016GB005567.

Received 3 NOV 2016
Accepted 3 MAR 2017
Accepted article online 7 MAR 2017
Published online 18 APR 2017

N_2O production and consumption from stable isotopic and concentration data in the Peruvian coastal upwelling system

Annie Bourbonnais[1], Robert T. Letscher[2], Hermann W. Bange[3], Vincent Échevin[4], Jennifer Larkum[1], Joachim Mohn[5], Naohiro Yoshida[6,7], and Mark A. Altabet[1]

[1]School for Marine Science and Technology, University of Massachusetts Dartmouth, New Bedford, Massachusetts, USA, [2]Earth System Science, University of California, Irvine, California, USA, [3]GEOMAR, Helmholtz Centre for Ocean Research Kiel, Kiel, Germany, [4]LOCEAN/IRD/IPSL, Laboratoire d'Océanographie et de Climatologie: Expérimentation et Approches Numériques, Paris, France, [5]Empa, Laboratory for Air Pollution and Environmental Technology, Dübendorf, Switzerland, [6]Department of Chemical Science and Engineering, Tokyo Institute of Technology, Yokohama, Japan, [7]Earth-Life Science Institute, Tokyo Institute of Technology, Tokyo, Japan

Abstract The ocean is an important source of nitrous oxide (N_2O) to the atmosphere, yet the factors controlling N_2O production and consumption in oceanic environments are still not understood nor constrained. We measured N_2O concentrations and isotopomer ratios, as well as O_2, nutrient and biogenic N_2 concentrations, and the isotopic compositions of nitrate and nitrite at several coastal stations during two cruises off the Peru coast (~5–16°S, 75–81°W) in December 2012 and January 2013. N_2O concentrations varied from below equilibrium values in the oxygen deficient zone (ODZ) to up to 190 nmol L^{-1} in surface waters. We used a 3-D-reaction-advection-diffusion model to evaluate the rates and modes of N_2O production in oxic waters and rates of N_2O consumption versus production by denitrification in the ODZ. Intramolecular site preference in N_2O isotopomer was relatively low in surface waters (generally −3 to 14‰) and together with modeling results, confirmed the dominance of nitrifier-denitrification or incomplete denitrifier-denitrification, corresponding to an efflux of up to 0.6 Tg N yr^{-1} off the Peru coast. Other evidence, e.g., the absence of a relationship between ΔN_2O and apparent O_2 utilization and significant relationships between nitrate, a substrate during denitrification, and N_2O isotopes, suggest that N_2O production by incomplete denitrification or nitrifier-denitrification decoupled from aerobic organic matter remineralization are likely pathways for extreme N_2O accumulation in newly upwelled surface waters. We observed imbalances between N_2O production and consumption in the ODZ, with the modeled proportion of N_2O consumption relative to production generally increasing with biogenic N_2. However, N_2O production appeared to occur even where there was high N loss at the shallowest stations.

1. Introduction

N_2O is an atmospheric trace gas, mainly produced by microbial processes, that directly and indirectly affects climate. As a tropospheric greenhouse gas, it is ~300 times more potent than CO_2 on a per molecule basis [*Forster et al.*, 2007]. With a long atmospheric residence time (>100 years), N_2O produced at the planet's surface reaches the stratosphere where it acts as the main source of ozone-depleting nitric-oxide radicals [*Nevison and Holland*, 1997; *Ravishankara et al.*, 2009]. Microbial processes associated with nitrogen cycling are the dominant natural sources of N_2O, with those in the open ocean accounting for up to ~35% of global emissions [*Forster et al.*, 2007; *Freing et al.*, 2012; *Ciais et al.*, 2013]. Still, major uncertainties exist in the distribution and magnitude of marine N_2O production, as important source regions, such as coastal areas, remain poorly characterized [*Nevison et al.*, 1995, 2004].

N_2O is produced in oxic ocean waters as a by-product of nitrifying microbes through decomposition of hydroxylamine, an intermediate during ammonium (NH_4^+) oxidation to nitrite (NO_2^-) as well as by nitrifier-denitrification, the sequential reduction of NO_2^- to N_2O [*Frame and Casciotti*, 2010] (Figure 1). Accordingly, there are strong positive correlations between apparent oxygen utilization (AOU) and excess N_2O or ΔN_2O (i.e., the difference between N_2O measured and at equilibrium) and NO_3^- concentrations [*Yoshinari*, 1976; *Cohen and Gordon*, 1979; *Nevison et al.*, 2003]. N_2O production yield from nitrification by

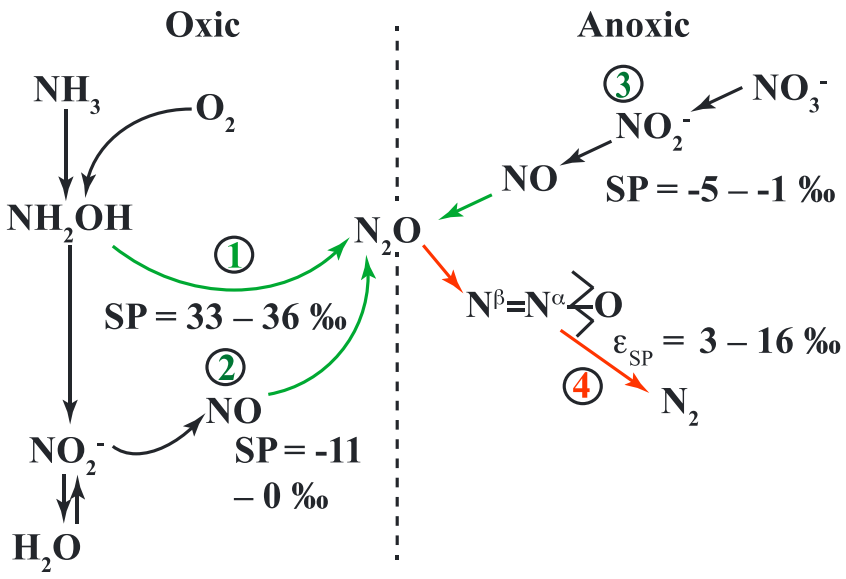

Figure 1. Microbial processes involved in marine N_2O production (green) and consumption (red) under oxic ($[O_2] > 5\ \mu mol\ L^{-1}$) and anoxic ($[O_2] < 5\ \mu mol\ L^{-1}$) conditions and associated SPs. The numbers represent N_2O production by (1) hydroxylamine oxidation, (2) nitrifier-denitrification, and (3) denitrifier-denitrification. N_2O conversion to N_2 during denitrification is the only process consuming N_2O (4).

either ammonia oxidizing Archaea or Bacteria is generally low, varying from 0 to 2% of NO_3^- production [*Yoshida et al.*, 1989; *Frame and Casciotti*, 2010; *Santoro et al.*, 2010, 2011; *Löscher et al.*, 2012] but has been argued to be enhanced under low-O_2^- conditions from both culture and field observations (up to 10% at low O_2 [*Goreau et al.*, 1980; *Ji et al.*, 2015]). However, other studies have not found such an enhancement [*Frame and Casciotti*, 2010].

Under anoxic conditions, N_2O may be both produced and consumed during denitrification, the sequential reduction of NO_3^-, NO_2^-, NO, to N_2O. N_2O in turn is reduced to nonbioavailable N_2 (Figure 1). The intermediate NO appears to remain mostly intracellular while NO_2^- and N_2O are able to exchange with external pools in the water column. Consequently, in the secondary NO_2^- maximum in oxygen deficient zone (ODZ), N_2O is generally near or below atmospheric equilibrium concentrations as a consequence of net removal [*Bange et al.*, 2001; *Yamagishi et al.*, 2007; *Babbin et al.*, 2015; *Kock et al.*, 2016]. Note that the biochemical pathway from NO_2^- to N_2O used by denitrifiers in anoxic waters is very similar to the nitrifier-denitrifier pathway in oxic waters.

The highest oceanic concentrations of N_2O and fluxes to the atmosphere have been reported from shallow suboxic waters overlying ODZs of the Indian Ocean, Eastern Tropical North Pacific (ETNP), and Eastern Tropical South Pacific (ETSP) [*Naqvi et al.*, 2000; *Arévalo-Martínez et al.*, 2015; *Babbin et al.*, 2015]. For instance, *Arévalo-Martínez et al.* [2015] observed the highest N_2O accumulations, up to 1 $\mu mol\ L^{-1}$, in surface waters off Peru. These high N_2O accumulations appear to form with changes from anoxic ($O_2 = 0\ \mu mol\ L^{-1}$) to suboxic ($O_2 < 5\ umol\ L^{-1}$) conditions as denitrifying waters are upwelled. A decoupling between N_2O production and its reduction to N_2 by denitrification, the latter process being less oxygen tolerant [*Dalsgaard et al.*, 2014], has been considered responsible for elevated N_2O concentrations near the oxycline [*Babbin et al.*, 2015; *Ji et al.*, 2015; *Kock et al.*, 2016].

Stable isotopes are widely used as natural tracers of N-cycle processes in the ocean integrating over their characteristic time and space scales [e.g., *Altabet*, 2006; *Sigman et al.*, 2005; *Bourbonnais et al.*, 2009, 2015]. Furthermore, natural stable isotope approaches do not suffer from the recognized problems of conventional inhibitor and tracer rate studies including incomplete diffusion of added tracers or inhibitors, alteration of microbial activity due to tracer substrate addition, or other unconstrained bottle effects [*Ostrom and Ostrom*, 2011].

Table 1. Compilation of Isotope Effects and Signatures for N_2O Production and Consumption (in ‰), i.e., N_2O Reduction to N_2[a]

$^{15}\varepsilon$	$^{18}\varepsilon$	SP	Condition	Reference
N_2O Production by Nitrification				
Nitrifier-Denitrification				
$NH_4^+ \rightarrow N_2O$				
58 ± 4	−8 ± 1	−11 ± 3	*Nitrosomonas marina*	*Frame and Casciotti* [2010]
$NO_2^- \rightarrow N_2O$				
–	–	0 ± 2	*Nitrosospira multiformis*	*Sutka et al.* [2006]
31–40	−12 – −7	−1 ± 6	*Nitrosomonas europaea*	*Sutka et al.* [2003, 2004]
Hydroxylamine Oxidation				
$NH_4^+ \rightarrow N_2O$				
–	3 ± 1	36 ± 2	*Nitrosomonas marina*	*Frame and Casciotti* [2010]
47	–	31 ± 4	*Nitrosomonas europaea*	*Sutka et al.* [2006]
$NH_2OH \rightarrow N_2O$				
−2	–	34 ± 1	*Nitrosomonas europaea*	*Sutka et al.* [2006]
−2	–	33 ± 1	*Nitrosospira multiformis*	*Sutka et al.* [2006]
−6	–	36 ± 1	*Methylosinus trichosporium*	*Sutka et al.* [2006]
−5–0	−61 – −54	31 ± 6	*Methylococcus capsulatus*	*Sutka et al.* [2003, 2004]
7 ± 2[b]	–	30 ± 1[b]	*Candidatus Nitrosopelagicus brevis CN25*	*Santoro et al.* [2011]
Abiotic Oxidation				
–	–	34–36		*Heil et al.* [2014]
–	–	30 ± 2		*Toyoda et al.* [2005]
N_2O Production by Denitrification				
$NO_3^- \rightarrow N_2O$				
13	–	−1 ± 2	*Pseudomonas chlororaphis*	*Sutka et al.* [2006]
37	–	−1 ± 2	*Pseudomonas aureofaciens*	*Sutka et al.* [2006]
10–22	−23 – −4	−5 ± 2	*Paracoccus denitrificans*	*Toyoda et al.* [2005]
29 ± 2	–	–	*Paracoccus denitrificans*	*Barford et al.* [1999]

$^{15}\varepsilon$	$\varepsilon\alpha$	$\varepsilon\beta$	$^{18}\varepsilon$	εSP		
N_2O Consumption by Denitrification						
$N_2O \rightarrow N_2$						
4–8	6–10	2–6	13–19	3–5	soil	*Jinuntuya-Nortman* [2008]
4	7	2	11	5	*Pseudomonas stutzeri*	*Ostrom et al.* [2007]
7	9	2	15	7	*Pseudomonas denitrificans*	*Ostrom et al.* [2007]
12 ± 1	20 ± 2	3 ± 0	31 ± 3	16 ± 2	ETNP (advection-diffusion-reaction model)	*Yamagishi et al.* [2007]
7–10	–	–	13–25	–	soil	*Menyailo and Hungate* [2006]
6–8	–	–	16–21	–	soil	*Menyailo and Hungate* [2006]
2	–	–	5	–	landfill soil	*Mandernack et al.* [2000]
13	–	–	–	–	*Pseudomonas denitrificans*	*Barford et al.* [1999]

[a]See Figure 1 for complete reactions.
[b]The exact mechanism, isotope effects and SP for N_2O production by Archaea are still not well constrained.

The N_2O molecule is uniquely rich in information from stable isotopic composition, containing both bulk ($\delta^{15}N$ and $\delta^{18}O$) and ^{15}N site specific signatures that are valuable for identifying production and consumption processes. Bulk $\delta^{15}N$ and $\delta^{18}O$ are expressed as

$$\delta^{15}\mathrm{N} \text{ or } \delta^{18}\mathrm{O} = \left(\left(R_{\mathrm{sample}}/R_{\mathrm{reference}}\right)\text{-}1\right) \times 1000 \quad (1)$$

Units are in parts per thousand or per mil (‰), and R is the ratio of $^{15}N/^{14}N$ or $^{18}O/^{16}O$. Reference materials are atmospheric N_2 for N (scale AIR-N_2) and mean ocean water for O (scale Vienna standard mean ocean water, VSMOW). Site preference (SP) is calculated from the difference in $\delta^{15}N$ between the central (α) and outer (β) N atoms in the linear, asymmetrical N_2O molecule (NNO):

$$\mathrm{SP} = \delta^{15}\mathrm{N}^{\alpha} - \delta^{15}\mathrm{N}^{\beta} \quad (2)$$

Nonzero SP arises from the differential biochemical bond making and breaking experienced by each of the two N atoms as a consequence of their different molecular positions (Figure 1). For example, in the consumption of N_2O by denitrification, the bond between the O atom and the α N atom is broken. It would then be expected that any isotopic fractionation occurring during this process would mostly influence the α position $^{15}N/^{14}N$ ratio thereby increasing the SP of the residual population of N_2O molecules.

The bulk isotopic composition ($\delta^{15}N$ and $\delta^{18}O$) of N_2O depends in part on the isotopic composition of its substrates (Figure 1). In the case of hydroxylamine oxidation, bulk N_2O $\delta^{15}N$ and $\delta^{18}O$ are functions of the $\delta^{15}N$ of the source NH_4^+ and $\delta^{18}O$ of dissolved O_2, respectively. For nitrifier-denitrification and denitrification, N_2O $\delta^{15}N$ and $\delta^{18}O$ is dependent on the $\delta^{15}N$ and $\delta^{18}O$ of source NO_3^- and/or NO_2^-. A further consideration is that significant O exchange usually occurs between NO_2^- and H_2O during N_2O production by nitrifier-denitrification or denitrification [*Wrage et al.*, 2005; *Kool et al.*, 2011; *Snider et al.*, 2012], which would decouple the $\delta^{18}O$ values of source and product.

Isotopic fractionation during nitrification and denitrification is the other major influence on the $\delta^{15}N$ and $\delta^{18}O$ of N_2O. Kinetic isotope fractionation occurs as a consequence of differences in reaction rate for the isotopologues of a molecule (e.g., ^{14}N, ^{15}N and ^{16}O, ^{18}O for N_2O). Typically, the molecules containing the lighter isotopes react more quickly leaving the residual substrate enriched in heavier isotopes (e.g., ^{15}N and ^{18}O). The isotope effect (ε) is defined here by

$$\varepsilon = ((k_1/k_2)\text{-}1) \times 1000 \quad (3)$$

where k_1 and k_2 are the reaction rates for the lighter and heavier isotopes, respectively.

N and O isotope effects for ($^{15}\varepsilon$, $^{18}\varepsilon$) during N_2O production and consumption vary substantially in laboratory culture as well as in the environment, likely as a result of sensitivity to growth conditions and reaction rates [*Lewicka-Szczebak et al.*, 2015] and perhaps unconstrained variations in substrate isotopic composition (Table 1). Of course, such variability can complicate the interpretation of field data.

In contrast to bulk isotope values, N_2O SP is independent of the initial isotopic composition of the substrate [*Toyoda et al.*, 2002; *Schmidt et al.*, 2004]. Thus, SP is only process-dependent and can be used as a robust tracer to identify the source of N_2O. For instance, low SP isotopic signatures (−11 to 0‰) are associated with N_2O production via NO_2^- reduction by nitrifier-denitrification or denitrification. Much higher SP values are indicative of N_2O production by hydroxylamine oxidation (30–36‰) [*Sutka et al.*, 2006; *Frame and Casciotti*, 2010]. However, SP does increase as a result of isotope fractionation during consumption by denitrification as discussed above [*Yamagishi et al.*, 2005, 2007; *Ostrom et al.*, 2007].

The main goal of this study is to identify the primary sources and sinks for N_2O in coastal waters of the ETSP using a natural stable isotope approach. In particular, we seek to understand the processes leading to near-surface, high N_2O concentrations that could contribute to high fluxes to the atmosphere. We present N_2O concentrations; isotope and isotopomer data for N_2O, NO_3^-, and NO_2^-, and other complementary physical and chemical parameters at two high-resolution coastal transects sampled off the coast of Peru in December 2012 (transect A) and January 2013 (transect B, Figure 2). We also used a 3-D-reaction-advection-diffusion regional box model to diagnose physical mixing and biological N_2O fluxes from the field data and evaluate the contribution from different N_2O production processes in oxic and low-O_2 waters and N_2O consumption versus production in the ODZ.

2. Materials and Methods

2.1. Sample Collection and Hydrographic Data

Samples were collected during two research cruises aboard the R/V *Meteor* on 2 to 23 December 2012 (M91) and 5 to 31 January 2013 (M92) (Figure 2), as part of the German projects SFB 754 (Climate-Biogeochemistry Interactions in the Tropical Ocean) and SOPRAN (Surface Ocean Processes in the Anthropocene). Water samples were collected by using 12 L Niskin bottles (~23 depths per profile) on a conductivity-temperature-depth (CTD) rosette equipped with pressure, conductivity, temperature, and oxygen sensors. Oxygen and nutrient (NO_3^-, NO_2^-, NH_4^+, and PO_4^{3-}) concentrations were measured on board as described in *Stramma et al.* [2013].

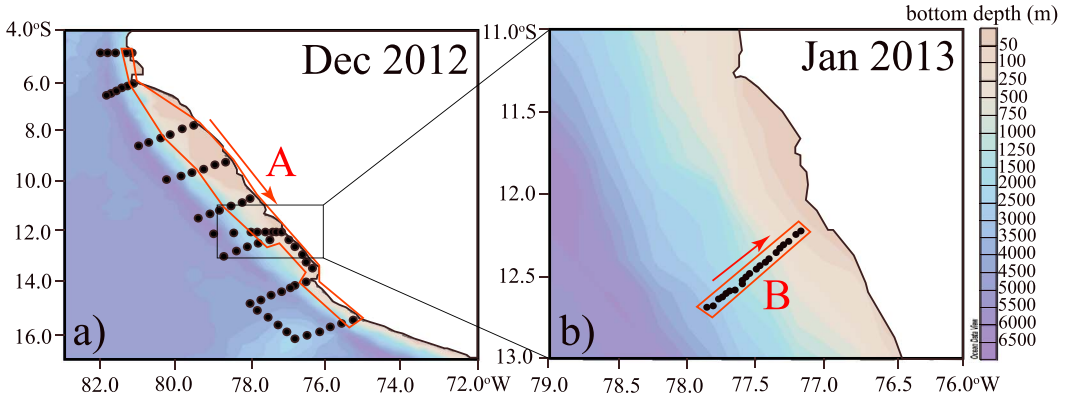

Figure 2. Maps showing stations sampled (black dots) during the (a) M91 cruise in December 2012 and (b) M92 cruise in January 2013. The two coastal transects (A and B, red rectangles) used for our analysis are shown.

Samples for dissolved N_2O were collected in a similar fashion as for dissolved $O_2/N_2/Ar$ samples [see *Charoenpong et al.*, 2014]. Tygon tubing was attached to the Niskin bottle, and a 165 mL serum glass bottle was filled and overflowed with seawater at least 2 times before capping with a butyl stopper and crimp sealed with aluminum seal. This procedure was executed underwater in a plastic container to avoid air bubbles. After collection, 0.2 mL of a saturated $HgCl_2$ solution was injected to prevent biological activity.

Samples for N_2/Ar were collected similarly in 60 mL serum glass bottles and preserved with 100 μL $HgCl_2$ [*Charoenpong et al.*, 2014]. Duplicate N_2/Ar samples were collected at every other depth.

Samples for N and O isotopic composition of NO_3^- were collected in 125 mL plastic bottles and acidified for preservation (1 mL of 2.5 mM sulfamic acid in 25% HCl), which also served to remove NO_2^- at the time of sample collection [*Granger and Sigman*, 2009]. For NO_2^- isotopic analysis, samples were collected and preserved with NaOH (2.25 mL of 6 M NaOH in 125 mL, pH = 12.5) to prevent oxygen isotope exchange with water during storage [*Casciotti et al.*, 2007]. Samples were stored at room temperature before analysis.

2.2. N_2O Concentrations, Isotopes, and Isotopomers

Analyses were made by using a GV IsoPrime Continuous Flow, MultiCollector, Isotope-Ratio Mass Spectrometer (CF-MC-IRMS) coupled to an automated gas extraction similar to what is used for $O_2/N_2/Ar$ samples [*Charoenpong et al.*, 2014], with some modifications. Our IRMS has the necessary collector configuration for simultaneous determination of masses 30, 31 for the NO^+ fragment of N_2O (determination of $\delta^{15}N^{\alpha}$) and 44, 45, and 46 (determination of $\delta^{15}N^{bulk}$ and $\delta^{18}O$).

Briefly, seawater is pumped from sample bottles through a gas-extractor that is continuously sparged with He. Dissolved N_2O was completely extracted into the He continuous flow and concentrated and purified in a purge-trap system. CO_2 is chemically removed, and H_2O vapor is eliminated with both chemical and cryogenic traps. N_2O is cryofocused with two liquid N_2 traps and passed through a capillary gas chromatography (GC) column prior to IRMS analysis. These latter steps are nearly identical to those used by *McIlvin and Casciotti* [2010] including GC column backflushing to eliminate interferences in the SP determination. For standardization, aliquots of gas standards are injected upstream of the gas-extractor to "experience" all extraction and purification steps.

We calibrated our measurements and corrected for scrambling between the α and β positions [*Westley et al.*, 2007] using N_2O standards covering a large range of SP (as well as $\delta^{15}N^{bulk}$ and $\delta^{18}O$) composition (Table 2) [see *Mohn et al.*, 2014]. These standards were analyzed in duplicate for each run to quantify the scrambling effect and potential offsets, and we iteratively solved for the different calibration parameters as described in *Frame and Casciotti* [2010] and *Mohn et al.* [2014]. Correction for isobaric interference from ^{17}O is included in these procedures. We have optimized water and He flows to achieve quantitative extraction and reproducibility of results even at low N_2O concentration (down to ~5 nmol L^{-1}). Instrumental drift was determined from measurements of the 5°C seawater standard distributed throughout an analytical run.

Standard deviations for triplicate measurements of our N_2O standards were typically below 0.1‰ for $\delta^{15}N^{bulk}$-N_2O, 0.1‰ for $\delta^{18}O$-N_2O, and 1.0‰ for SP, which are comparable to values reported by *Mohn et al.* [2014].

Table 2. N_2O, NO_3^-, and NO_2^- Standards Used for Sample Calibration (in ‰)

	$\delta^{15}N^{\alpha}$	$\delta^{15}N^{\beta}$	$\delta^{18}O$	$\delta^{15}N^{bulk}$	SP
			N_2O		
EMPA CB0897	15.7	−3.21	35.2	6.245	18.91
EMPA CB0971	−82.1	−78	21.6	−80.05	−4.1
EMPA CB0976	5.55	−12.9	32.7	−3.675	18.45
EMPA 5350	1.71	94.4	36	48.055	−92.69
			NO_3^-		
	$\delta^{15}N$			$\delta^{18}O$	
IAEA N3	4.7			25.6	
USGS 34	−1.8			−27.9	
USGS 35	2.7			57.5	
LABmix[a]	38.9			–	
			NO_2^-		
	$\delta^{15}N$			$\delta^{18}O$	
MAA1[a]	−60.6			–	
MAA2[a]	3.9			–	
Zh1[a]	−16.4			–	
N23	3.7			11.4	
N7272	−79.6			4.5	
N10219	2.8			88.5	

[a]In house standard.

N_2O concentrations in our samples were calculated from relative peak heights between the samples and a seawater standard of known N_2O concentration equilibrated with the atmosphere at 5°C (12.5 nmol L^{-1} at salinity 34 as calculated by using the *Weiss and Price*'s [1980] equation). Equilibrium N_2O concentrations were calculated by using the global mean contemporary atmospheric N_2O dry mole fraction of 325 ppb in December 2012 and January 2013 (http://agage.mit.edu/data/agage-data). We observed close agreement between the N_2O concentrations measured with our IRMS and those measured independently by *Kock et al.* [2016] by using gas chromatography and an electron capture detector.

2.3. Biogenic N_2

N_2/Ar and $\delta^{15}N$-N_2 measurements were made on septum-sealed samples by using an online gas extraction system coupled to a CF-MC-IRMS as described in *Charoenpong et al.* [2014]. Excess N_2 concentration ($[N_2]_{excess}$) in μmol L^{-1}, the observed $[N_2]$ minus the equilibrium $[N_2]$ at in situ temperature and salinity, was calculated as in *Charoenpong et al.* [2014] and calibrated daily against seawater standards equilibrated with air at fixed temperature. Standard deviation for the samples was generally better than 0.7 μmol L^{-1} for $[N_2]_{excess}$. We calculated biogenic $[N_2]$ ($[N_2]_{biogenic}$), the $[N_2]$ produced by denitrification or anammox, by subtracting the $[N_2]_{excess}$ at a background station unaffected by N loss from the observed $[N_2]_{excess}$ at corresponding potential density, as in *Bourbonnais et al.* [2015]. This corrects for nonregional biological N loss as well as physically produced deviations in equilibrium N_2/Ar [*Hamme and Emerson*, 2002].

2.4. N and O Isotopic Composition of NO_3^- and NO_2^-

The stable isotopic compositions ($\delta^{15}N$ and $\delta^{18}O$) of NO_3^- and NO_2^- were analyzed by using the "bacteria method" [*Sigman et al.*, 2001; *Casciotti et al.*, 2002] and the "azide method" [*McIlvin and Altabet*, 2005]. For NO_3^- isotopic analysis, samples were neutralized and NO_3^- was quantitatively converted to N_2O by cultured denitrifying bacteria that lack the active N_2O-reductase enzyme (*Pseudomonas chlororaphis*, ATCC #13985) [*Casciotti et al.*, 2002]. Blank contribution was generally below 5% of the target sample size. For NO_2^- isotopic analysis, NO_2^- was converted to nitrous oxide (N_2O) by using sodium azide in acetic acid. The reagent was modified by increasing the acetic acid concentration to 7.84 M to account for high sample pH. N_2O gas was automatically extracted, purified, and analyzed online by using a purge-trap preparation system coupled to an IsoPrime CF-IRMS. Standard sample size was 20 nmol N_2O for NO_3^- isotope analysis and 15 nmol N_2O for NO_2^- isotope analysis. N and O isotope ratios are reported in per mil (‰), relative to AIR-N_2 for $\delta^{15}N$ and to VSMOW for $\delta^{18}O$ as in equation (1).

NO_3^- and NO_2^- isotope data were calibrated by using the reference materials listed in Table 2 [see *Casciotti and McIlvin*, 2007]. The reproducibility was generally better than 0.2‰ for $\delta^{15}N$ and 0.5‰ for $\delta^{18}O$ in NO_3^- and NO_2^-.

2.5. Regional Box Model Description

We diagnosed the biological fluxes and ratios of N_2O production and consumption processes from the observational data. We accounted for the fluid flow field and physical mixing of N_2O and its isotopomers within

regional box models spanning the spatiotemporal scales of our cruise collected data (see Figure S1 in the supporting information). The physical mixing was estimated by using physical circulation output from an eddy-resolving ROMS (Regional Ocean Modeling System [*Shchepetkin and McWilliams*, 2005]) simulation. The ROMS model has been used to represent the regional mesoscale circulation in the Peru region with a model configuration similar to that in *Penven et al.* [2005]: it has a 1/9° × 1/9° spatial resolution (~12 km) and 32 vertical levels with a refined vertical resolution near the surface. For more details on the model configuration, the reader is referred to *Penven et al.* [2005]. This model has been validated against observations in previous works [e.g., *Echevin et al.*, 2011; *Montes et al.*, 2011; *Pietri et al.*, 2014]. Temperature and potential density simulated from the ROMS and observed during both the M91 and M92 cruises agreed well (Figure S2). In the present study, it was forced by monthly open boundary conditions from the 1/4° GLORYS2V3 reanalysis over the period of 2007–2013 operated by Mercator-Ocean and downloaded on the Copernicus platform (http://marine.copernicus.eu). Advanced scatterometer daily wind stress processed by Centre ERS d'Archivage et de Traitement (http://cersat.ifremer.fr/), climatological heat and freshwater fluxes from Comprehensive Ocean-Atmosphere Data Set [*Da Silva et al.*, 1994], and a restoring of sea surface temperature to advanced very high resolution radiometer optimum interpolation sea surface temperature daily data following *Barnier et al.* [1995], were used at the ocean-atmosphere model interface.

A 70-box model was constructed to encompass the 56 stations sampled for N_2O and its isotopomers during the M91 cruise in December 2012. The 70-box model has dimensions 7 (lat) × 2 (lon) × 5 (depth), spanning 5–16°S, oriented at an angle of ~ −45° from north, which aligns the boxes with the Peru coastline (Figure S3). The longitudinal line separating the inshore (overlying the shelf) boxes from the offshore boxes follows the 300 m isobath. The top of depth level 1 (see Figure S3) begins below the surface mixed layer at 10 m depth as to ignore sea-air gas exchange of N_2O with the atmosphere.

A 25-box model was constructed to encompass the 13 stations sampled for N_2O and its isotopomers during the M92 cruise in January 2013. The 25-box model has dimensions 5 (lon) × 5 (depth, spanning 5–900 m) in the region covering 12.2 to 12.8°S and 77.0 to 77.9°W, oriented at an angle of ~ +45° from north, which aligns the boxes perpendicular with the Peru coastline (Figure S4).

Observed $[N_2O]$, $\delta^{15}N^{\alpha}$-N_2O, and $\delta^{15}N^{\beta}$-N_2O were interpolated onto the box model grid and averaged when multiple observations were included in a given model box. Physical mixing of N_2O and its isotopomers by horizontal advection, vertical advection (upwelling), and vertical diffusion between model boxes were considered by using output from a regional ROMS simulation for the months of December 2012 and January 2013. Three-day averaged output of the **u**, **v**, and **w** velocities (m/s) as well as the log-transformed vertical diffusivity coefficient (k_z; m^2/s) were time averaged to obtain the monthly averaged circulation properties. The 1/9° resolution ROMS output, which lies on a terrain-following (sigma) vertical grid, was interpolated onto the box model grid and averaged for a given model box. Advective velocities and vertical diffusivity were combined with $[N_2O]$ and its isotopomer gradients to compute the physical mixing of tracers between model boxes as

$$\frac{\partial [N_2O]_{phy}}{\partial t} = \nabla u N_2O + \frac{\partial}{\partial z} w N_2O + \frac{\partial}{\partial z} kz \frac{\partial}{\partial z} N_2O \tag{4}$$

$$\frac{\partial \left(\delta^{15}N^{\alpha} \times [N_2O]\right)_{phy}}{\partial t} = \nabla \left(u \times \delta^{15}N^{\alpha} \times N_2O\right) + \frac{\partial}{\partial z}\left(w \times \delta^{15}N^{\alpha} \times N_2O\right) + \frac{\partial}{\partial z} kz \frac{\partial}{\partial z}\left(\delta^{15}N^{\alpha} \times N_2O\right) \tag{5}$$

with an equation analogous to equation (5) for mixing of $\delta^{15}N^{\beta}$-N_2O. Horizontal diffusion of tracers was not considered, as the ROMS model is eddy-resolving and does not include an explicit diffusion scheme except near the model domain open boundaries [*Penven et al.*, 2005]. The quantity $\partial[N_2O]_{phy}/\partial t$ was substituted into equations (6)–(9) below to solve for the biological rates producing or consuming N_2O. Anoxic versus oxic boxes in the model were determined by interpolating cruise observed dissolved $[O_2]$ onto the model grid by using a 5 μmol L^{-1} $[O_2]$ cutoff. Boundary fluxes were computed by using ROMS velocities and vertical diffusivity output for the regions immediately to the north, south, and west of the box model domain as well as above (0–10 m depth) and below (300–350 m depth or bottom). N_2O tracer data for the boundary fluxes were taken from the northernmost, southernmost, or westernmost stations as well as the mixed layer (0–10 m) and at depth (>300 m) where available.

The following equations describing the biological fluxes of N_2O and its isotopomers were used in shallow oxic waters ($[O_2] > 5\ \mu mol\ L^{-1}$):

$$\frac{\partial[N_2O]_{box}}{\partial t} = \frac{\partial[N_2O]_{ND}}{\partial t} + \frac{\partial[N_2O]_{HO}}{\partial t} + \frac{\partial[N_2O]_{phy}}{\partial t} \quad (6)$$

$$\left(SP_{box} \times \frac{\partial[N_2O]_{box}}{\partial t}\right) = \left(SP_{ND} \times \frac{\partial[N_2O]_{ND}}{\partial t}\right) + \left(SP_{HO} \times \frac{\partial[N_2O]_{HO}}{\partial t}\right) + \left(\frac{\partial(SP \times [N_2O])_{phy}}{\partial t}\right) \quad (7)$$

where $\partial[N_2O]_{box}/\partial t$ is the rate of N_2O concentration change for a given model box (sum of biological + mixing terms); SP_{box} is the observed SP for a given box, $\partial[N_2O]_{ND}/\partial t$, $\partial[N_2O]_{HO}/\partial t$, SP_{ND}, and SP_{HO} are the fluxes and SPs from nitrifier-denitrification and hydroxylamine oxidation; and $\partial(SP \times [N_2O])_{phy}/\partial t$ represents the physical mixing flux of SP × $[N_2O]$ calculated as $\partial(\delta^{15}N^{\alpha} \times N_2O)/\partial t - \partial(\delta^{15}N^{\beta} \times N_2O)/\partial t$ (Table 1 and Figure S1).

The following equations were used for ODZ waters ($[O_2] < 5\ \mu mol\ L^{-1}$):

$$\frac{\partial[N_2O]_{box}}{\partial t} = \frac{\partial[N_2O]_{PD}}{\partial t} + \frac{\partial[N_2O]_{CD}}{\partial t} + \frac{\partial[N_2O]_{phy}}{\partial t} \quad (8)$$

$$\left(SP_{box} \times \frac{\partial[N_2O]_{box}}{\partial t}\right) = \left(SP_{PD} \times \frac{\partial[N_2O]_{PD}}{\partial t}\right) - \left((SP_{box} - \varepsilon_D) \times \frac{\partial[N_2O]_{CD}}{\partial t}\right) + \left(SP_{phy} \times \frac{\partial[N_2O]_{phy}}{\partial t}\right) \quad (9)$$

where $\partial[N_2O]_{PD}/\partial t$ and $\partial[N_2O]_{CD}/\partial t$ are the fluxes from N_2O production and consumption by denitrification, ε_D is the isotope effect for SP during denitrification consumption, and SP_{PD} is the SP for denitrification production (Table 1 and Figure S1).

The box model assumes steady state, such that the sum of all fluxes into/out of (mixing) or within a box (biological) equal zero.

3. Results

3.1. Distribution of O_2, Biogenic N_2, NO_3^- and NO_2^- Concentrations and Isotopes

Indicative of intense coastal upwelling, the mixed layer was always relatively shallow, i.e., ~5 m depth for transect A (Figure 3a), and less than 50 m depth at the deepest stations for transect B (Figure 4a). The oxycline ($[O_2] < 5\ \mu mol\ L^{-1}$), marking the upper ODZ boundary, became shallower from north to south along transect A varying from ~200 m at 6°S to ~20 to 50 m south of 10°S (Figures 3a and 4a). Along the outer shelf and slope, primary water masses were Antarctic Intermediate Water (AAIW; $S \approx 34.5$, $T = 5.5$°C) below 500 m and Equatorial Subsurface Water (ESSW; $34.7 < S < 34.9$, 8.5°C $< T < 10.5$°C) below the thermocline, with the latter corresponding to the low O_2 core of the southward flowing Peru-Chile Undercurrent (PUC) [*Strub et al.*, 1998]. Peru Coastal Waters (PCW; $S \approx 35.0$, $T < 19$°C; referred to as Cold Coastal Waters in *Pietri et al.* [2014]) were found next to the coast and mainly resulted from mixing between colder and slightly fresher upwelled waters from the PUC with Subtropical Surface Water (STSW; $S > 35$, 20°C $< T <$ 28°C) [*Strub et al.*, 1998] (Figure 5).

From north to south along transect A, subsurface waters reached the critically low levels of O_2 required for the onset of N-loss processes (Figure 3). Biogenic N_2 correspondingly increased as NO_3^- was consumed in the ODZ, with a maximum of ~20 $\mu mol\ L^{-1}$ at 35 m depth at station 63 (Figure 3c). Relatively high biogenic N_2 concentrations were also observed in near-surface shelf waters south of 5°S, consistent with upwelling of ODZ waters impacted by N loss (Figures 3a, 3c and 4a, 4c).

This increase in biogenic N_2 also corresponded to NO_2^- accumulations of up to 11 $\mu mol\ L^{-1}$ in the coastal ODZ (50 m depth, station 64, transect A; Figure 3b). However, both NO_2^- and NO_3^- were almost completely consumed ($<0.5\ \mu mol\ L^{-1}$) at the shallowest stations (station 63, transect A and station 9, transect B; Figures 3b and 4b), which evidently had the highest extent of N loss.

Nitrate $\delta^{15}N$ and $\delta^{18}O$ increased with substrate consumption following isotopic fractionation during assimilatory NO_3^- reduction by phytoplankton ($\varepsilon = 5$‰ [*Altabet*, 2001]) and dissimilatory NO_3^- reduction in the coastal ODZ ($\varepsilon = 15$ to 25‰ [*Brandes et al.*, 1998; *Voss et al.*, 2001; *Granger et al.*, 2004, 2008; *Bourbonnais*

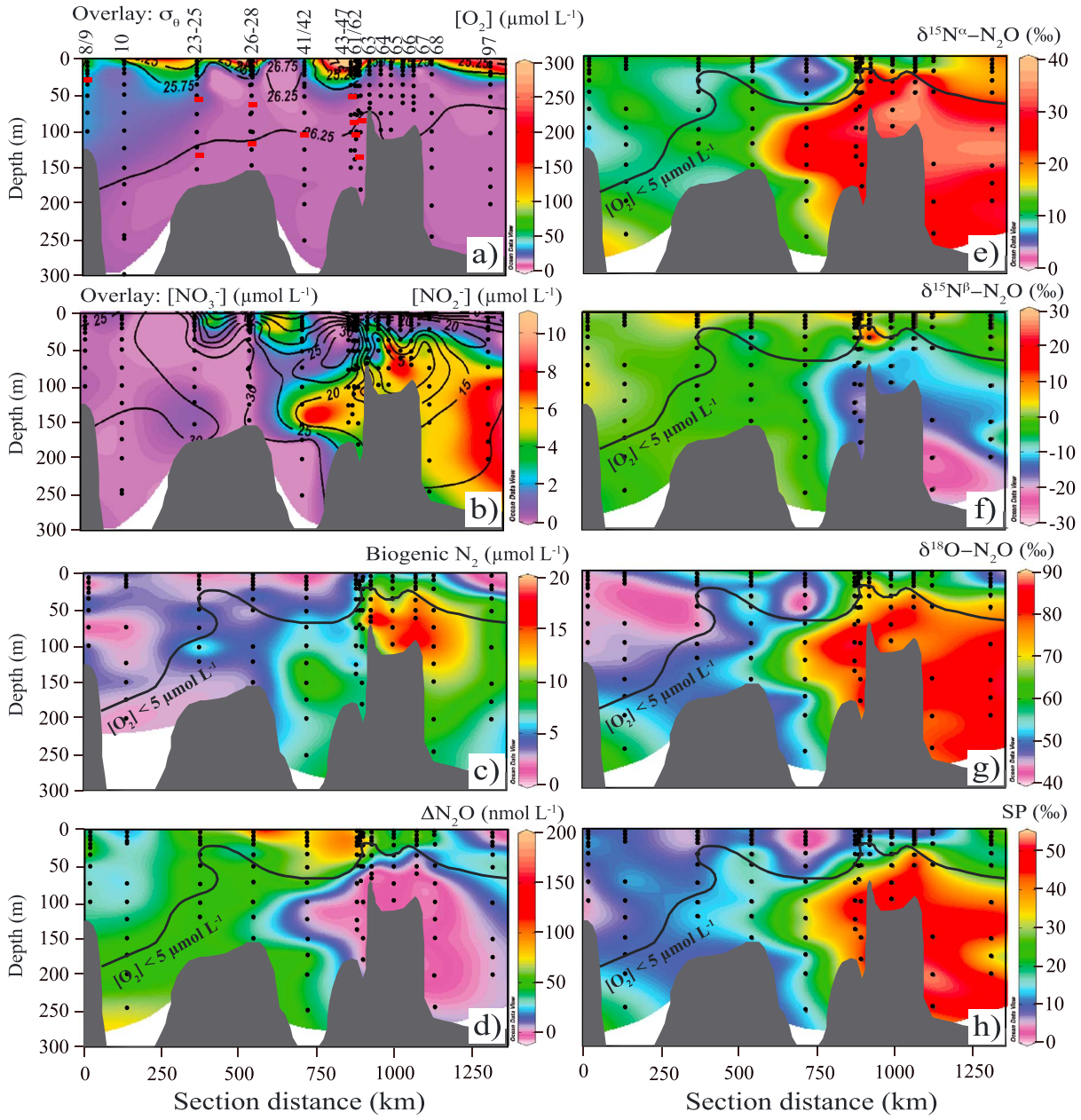

Figure 3. Key parameters for transect A along the Peru Coast (see Figure 2). (a) $[O_2]$ with σ_θ in overlay, (b) $[NO_2^-]$ with $[NO_3^-]$ in overlay, (c) biogenic N_2 (from N_2/Ar data), (d) ΔN_2O, (e) $\delta^{15}N^{\alpha}$-N_2O, (f) $\delta^{15}N^{\beta}$-N_2O, (g) $\delta^{18}O$-N_2O, and (h) SP. In Figure 3a, the depths of the different stations at a given latitude are indicated by red bars. Note that only one station was sampled for N_2O isotope and isotopomer analysis at a given latitude. CTD numbers are indicated at the top of Figure 3a. Bottom depth was ~300 m at the deepest station 10.

et al., 2015]) (Figures S5a and S5b). NO_2^- $\delta^{15}N$ also generally increased with substrate consumption, as expected during NO_2^- reduction ($\varepsilon = 8$ to 22‰ [*Bryan et al.*, 1983; *Brunner et al.*, 2013; *Bourbonnais et al.*, 2015]) (Figures S5c and S5d).

3.2. N_2O Concentrations and Isotopomers

During transects A and B, supersaturating N_2O concentrations as high as 180 nmol L^{-1} (station 26, transect A) occurred in oxygenated surface waters at a salinity of ~35 and temperature of ~15°C, characteristic of PCW [*Pietri et al.*, 2014; *Kock et al.*, 2016] (Figure 5) implying high potential fluxes to the atmosphere. In contrast, ΔN_2O in the anoxic ODZ decreased from ~60 nmol L^{-1} (station 10) to below saturating values (down to

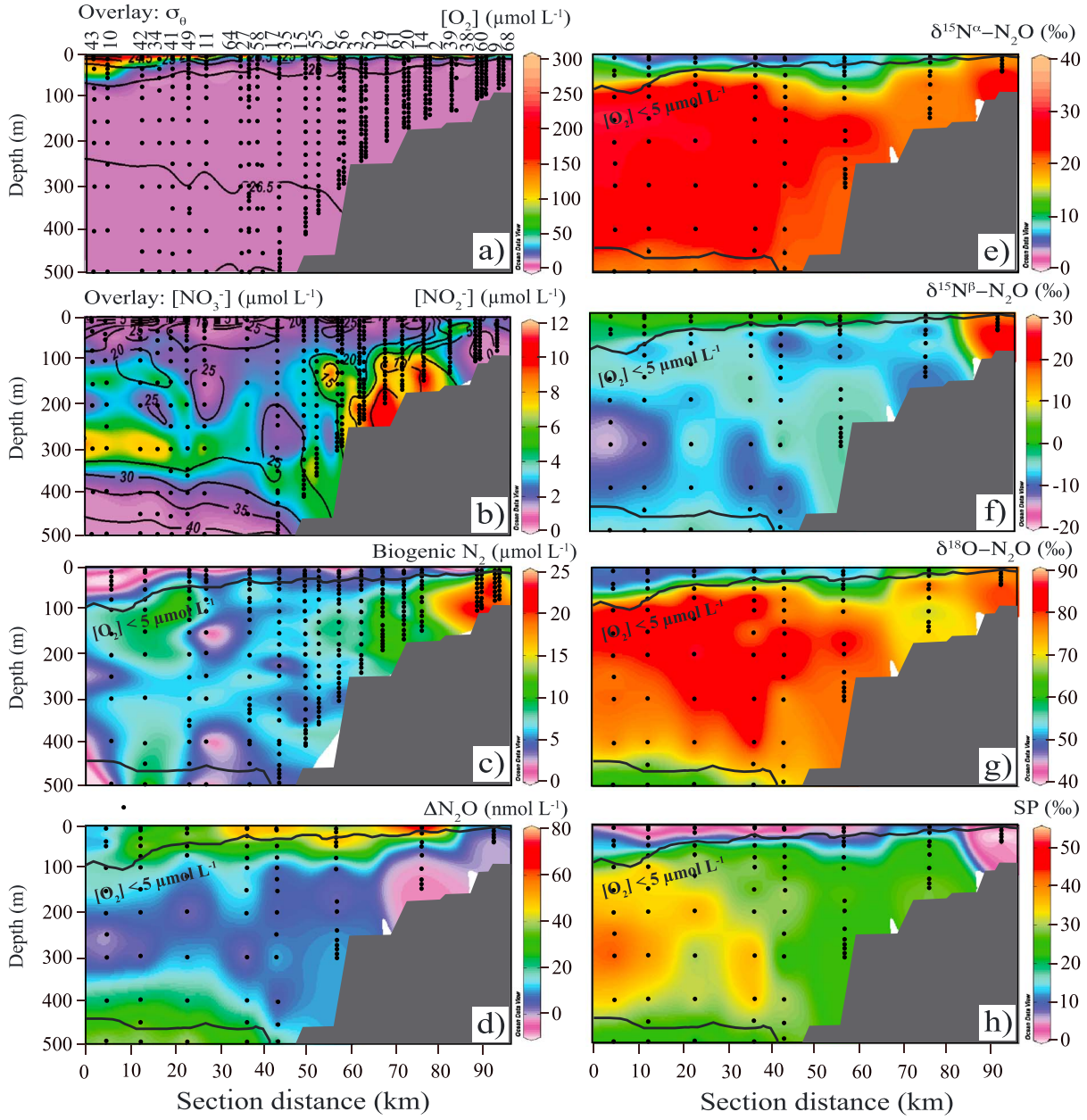

Figure 4. Key parameters for transect B normal to the Peru Coast (see Figure 2). (a) $[O_2]$ with σ_θ in overlay, (b) NO_2^-] with $[NO_3^-]$ in overlay, (c) biogenic N_2 (from N_2/Ar data), (d) ΔN_2O, (e) $\delta^{15}N^{\alpha}$-N_2O, (f) $\delta^{15}N^{\beta}$-N_2O, (g) $\delta^{18}O$-N_2O, and (h) SP. CTD numbers are indicated at the top of Figure 4a. Bottom depth was ~2000 m at the deepest station 43.

-7 nmol L^{-1} at station 63) as a consequence of net consumption by denitrification. South of 5°S, the region of low ΔN_2O expanded vertically along with the ODZ and was correlated with N loss (transect A; Figures 3c and 3d).

Some aspects of our observed coastal distribution of N_2O have also been found in offshore ODZ studies. North of 5°N in the ETSP a N_2O maximum of ~60 nmol L^{-1} was found in the oxygen minimum but further south a sharp double peak structure formed at the top and bottom of the ODZ with depletion within the core [*Cohen and Gordon*, 1978; *Law and Owens*, 1990; *Kock et al.*, 2016]. However, the shapes for the ΔN_2O in our near-coastal profiles were more variable and not as well defined as compared to offshore with significantly higher ΔN_2O above the oxycline.

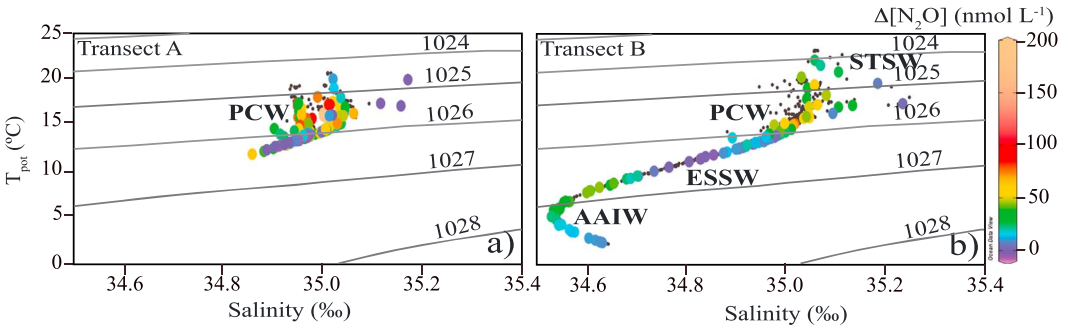

Figure 5. Temperature-salinity plots for transects A and B (Figure 2) with color-coded ΔN_2O (*z* axis). The grey lines represent σ_θ. Major water masses are indicated in bold (see section 3.1).

N_2O isotopomer composition varied widely along both transects A and B. In oxygenated near-surface waters throughout the study region ($[O_2] > 5\ \mu mol\ L^{-1}$), $\delta^{15}N^{\alpha}$-N_2O, $\delta^{15}N^{\beta}$-N_2O, $\delta^{18}O$-N_2O, and SP varied between 1 to 21‰, −5 to 10‰, 40 to 79‰, and −3 to 26‰, respectively (Figures 3, 4, and 6). The large range in $\delta^{18}O$-N_2O, in particular, was directly correlated with biogenic N_2 concentrations (transect A: $r^2 = 0.49$, p-value < 0.05, $n = 75$; transect B: $r^2 = 0.76$, p-value < 0.05, $n = 22$, at $O_2 > 5\ \mu mol\ L^{-1}$) and $\delta^{18}O$-NO_3^- (Figures 7c and 7d). In the ODZ, $\delta^{15}N^{\alpha}$-N_2O, $\delta^{18}O$-N_2O, and SP generally increased to up to 38‰, 93‰, and 56‰, respectively, as N loss increased with vertical expansion of the ODZ south of 5°S along transect A and toward the shelf (transect B). Interestingly, $\delta^{15}N^{\beta}$-N_2O generally remained the same or decreased as $\delta^{15}N^{\alpha}$-N_2O and biogenic N_2 increased in the coastal and offshore ODZs (Figures 3 and 4).

3.3. 3-D Reaction-Advection-Diffusion Box Modeling

The results from our regional box models showed high N_2O production rates of up to 49 nmol L^{-1} d^{-1} (transect B, Figures 8a and 8e) in oxic waters. These rates were generally higher than those measured by *Ji et al.* [2015] from ^{15}N-labeled incubations in offshore and coastal oxygenated waters in the ETSP (<1 nmol L^{-1} d^{-1}). N_2O production mainly occurred through nitrifier-denitrification (or incomplete denitrifier-denitrification as discussed below), which generally represented more than 50% of total N_2O production for transects A and B (Figures 8b and 8f and Tables S1 and S3 in the supporting information). N_2O production rates and the contribution from nitrifier (or incomplete denitrifier)-denitrification were also relatively high where the highest N_2O concentrations were observed (Figure 8).

In comparison, *Frame et al.* [2014] estimated that 64 to 68% of the N_2O production in the isotopic minimum of the upwelling zone off the southern African Coast was from nitrifier-denitrification using a simple model neglecting lateral and vertical advection/diffusion. Using a lower SP of −11‰ (as in *Frame et al.* [2014]) in our model decreased the contribution from nitrifier-denitrification (Tables S1 and S3). In addition, considering only vertical advection/diffusion generally decreased N_2O production rates with no clear effect on the partitioning between nitrifier-denitrification versus hydroxylamine oxidation (Tables S2 and S4). A major difference between both study areas is that in contrast to the upwelling zone off the African Coast, the coastal waters off Peru overlay an ODZ, and therefore, in addition to nitrifier-denitrification, N_2O production is also likely to occur through incomplete denitrifier-denitrification.

N_2O production rates in the ODZ derived from our box model were up to 13.5 nmol L^{-1} d^{-1} when assuming an SP of −0.5‰ for N_2O production by denitrifier-denitrification [*Sutka et al.*, 2006] and an isotope effect of either 5 or 16‰ [*Ostrom et al.*, 2007; *Yamagishi et al.*, 2007] for SP during N_2O consumption by denitrification (Tables S1 and S3). Our N_2O production rates were in the same order of magnitude as those estimated from ^{15}N-labeled incubations in the ETSP (up to ~4 nmol L^{-1} d^{-1} [*Ji et al.*, 2015]) and from a 1-D model neglecting lateral advection in the ETNP ODZs (2 to 35 nmol L^{-1} d^{-1} [*Babbin et al.*, 2015]). Measured N_2O consumption rates from tracer incubations by *Babbin et al.* [2015] in the ETNP ODZ balanced production and also agreed well with our modeled rates (up to ~40 nmol L^{-1} d^{-1}; Figures 8c and 8g).

N_2O consumption relative to production ranged from 12 to 96% for transect A and 0 to 100% for transect B (Figures 8d and 8h). Assuming a lower isotope effect of 5‰ for SP during N_2O consumption

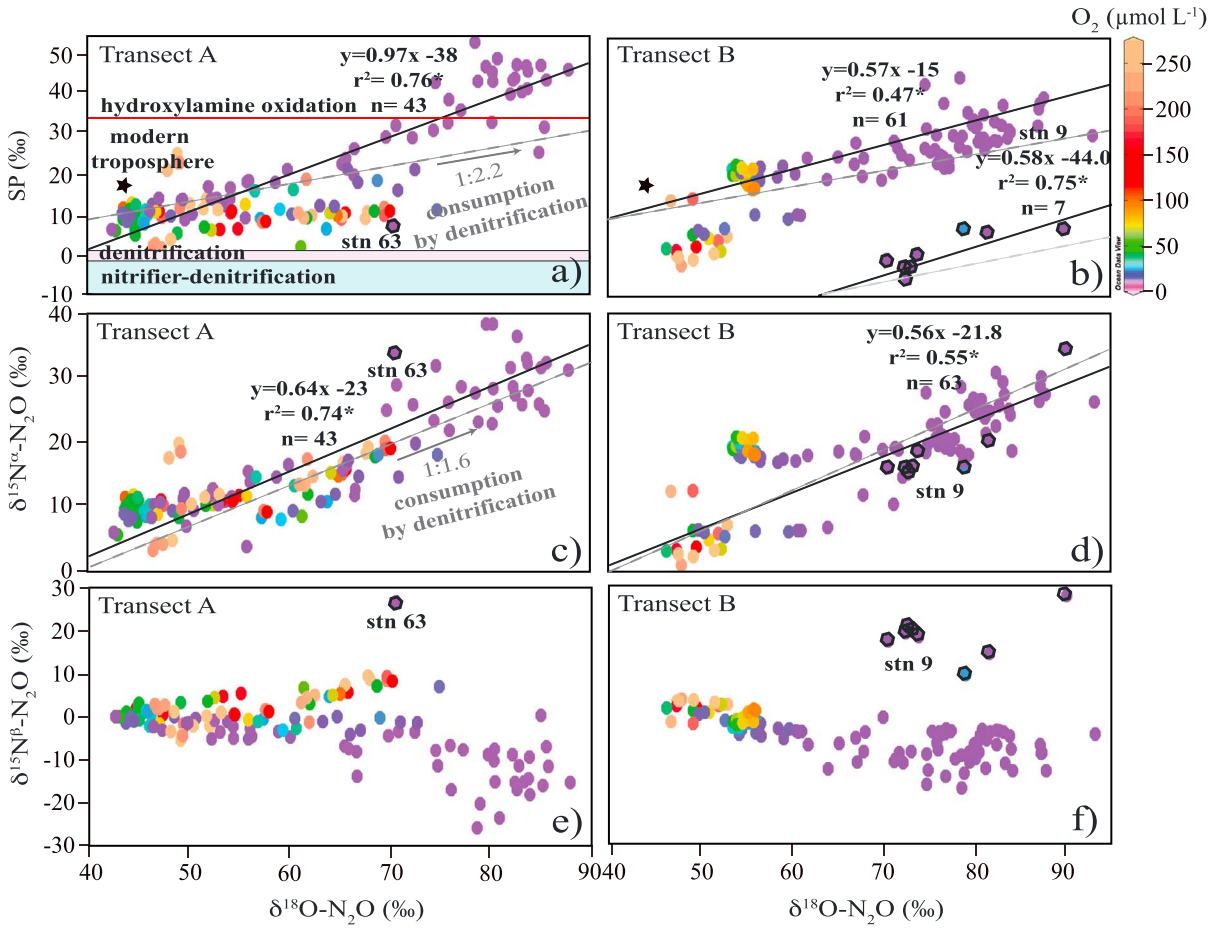

Figure 6. (a and b) SP versus δ^{18}O-N_2O, (c and d) $\delta^{15}N^{\alpha}$-N_2O versus δ^{18}O-N_2O and (e and f) $\delta^{15}N^{\beta}$-N_2O versus δ^{18}O-N_2O for coastal transects A and B with color-coded [O_2] (*z* axis). SP values for N_2O production by hydroxylamine oxidation, nitrifier-denitrification, and denitrification as well as for the modern troposphere (black stars [*Yoshida and Toyoda*, 2000]) are shown in Figures 6a and 6b. The pale grey dashed lines in Figures 6a–6d are the relationships between SP versus δ^{18}O-N_2O and $\delta^{15}N^{\alpha}$ versus δ^{18}O-N_2O expected during pure N_2O consumption by denitrification. The black lines are the linear regressions for samples with [O_2] < 5 µmol L^{-1}. Stars next to r^2 values indicate significant relationships. The hexagons are data points from stations 63 (transect A) and 9 (transect B) showing an increase in $\delta^{15}N^{\beta}$-N_2O with δ^{18}O-N_2O. Only shelf waters (<300 m depth for transect A and <500 m depth for transect B) were considered.

[*Ostrom et al.*, 2007] increased relative N_2O consumption. The highest relative N_2O consumption in our model also usually occurred at the highest extent of N loss, where N_2O concentrations were below equilibrium, except at the shallowest station 9 (transect B) (Figures 3, 4, and 8).

4. Discussion

4.1. Extreme ΔN_2O in Upwelling Waters Resulting From Incomplete Denitrification

Throughout most of the ocean, subsurface waters isolated from the atmosphere slowly accumulate N_2O as a by-product of nitrification with progressive organic matter remineralization and O_2 depletion. The subsurface intermediate waters entering the Peru coastal region in the form of the PUC have already experienced substantial organic matter remineralization since their formation in the Subantarctic and thus enter our study region already low in O_2 [*Strub et al.*, 1998] and elevated in N_2O. Hence, nitrification during the course of water mass aging both outside as well as within the study region, via either the hydroxylamine oxidation or nitrifier-denitrification [*Frame and Casciotti*, 2010] pathway is a likely source for positive ΔN_2O concentrations (up to ~180 nmol L^{-1}). This is particularly so for northern part of transect A which corresponds with the path of the southward flowing PUC. N_2O further accumulates in this portion of transect A where N_2O production is active, but no N_2O consumption occurs, in the absence of denitrification. An exception to this

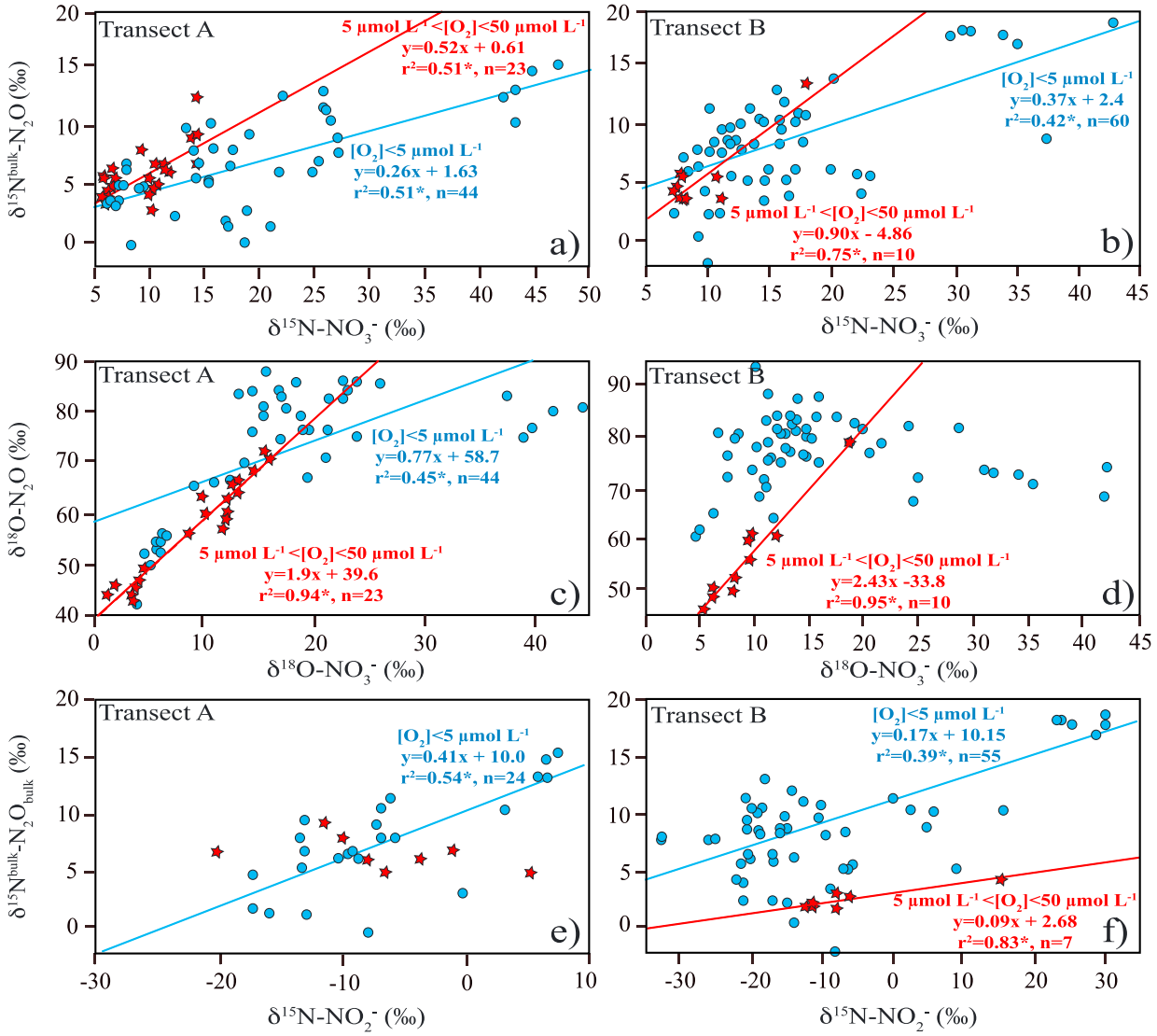

Figure 7. (a and b) δ^{15}N-NO_3^- versus $\delta^{15}N^{bulk}$-N_2O, (c and d) δ^{18}O-NO_3^- versus δ^{18}O-N_2O, and (e and f) δ^{15}N-NO_2^- versus $\delta^{15}N^{bulk}$-N_2O for transect A and B for $[O_2] < 5$ µmol L^{-1} (blue circles and lines) and 50 µmol $L^{-1} < [O_2] > 5$ µmol L^{-1} (red stars and lines). Only coastal waters (<500 m bottom depth) were considered. Stars next to r^2 values indicate significant relationships.

generality are instances of near-surface "hot spots" where incomplete denitrification may lead to some of the highest ΔN_2O values observed, as upwelled ODZ waters become modestly oxygenated inhibiting N_2O reduction to N_2 [*Arévalo-Martínez et al.*, 2015; *Kock et al.*, 2016]. N_2O may also accumulate disproportionately in our study region where O_2 is low given the possibility of increasing yield of N_2O production from nitrification under low oxygen concentrations [*Goreau et al.*, 1980; *Ji et al.*, 2015].

As N_2O-SP is only pathway-dependent [e.g., *Sutka et al.*, 2006], it can be used as a robust indicator of source pathway in the absence of consumption by denitrification. Production by nitrifier-denitrification (as well as denitrification) is associated with low SP values of −11 to 0‰, whereas hydroxylamine oxidation produces higher N_2O-SP values of 30–36‰ [*Sutka et al.*, 2006; *Frame and Casciotti*, 2010] (Table 1). These laboratory results are mainly for bacterial ammonia oxidizers, whereas archaeal ammonia oxidizers, which are thought to be the dominant nitrifiers in the ocean [*Santoro et al.*, 2011; *Löscher et al.*, 2012], have been shown in culture to produce N_2O with a high SP of 26–29‰, consistent with a hydroxylamine pathway. However, it was suggested that Archaea could also produce N_2O through NO_2^- reduction with lower SP in the environment [*Santoro et al.*, 2011].

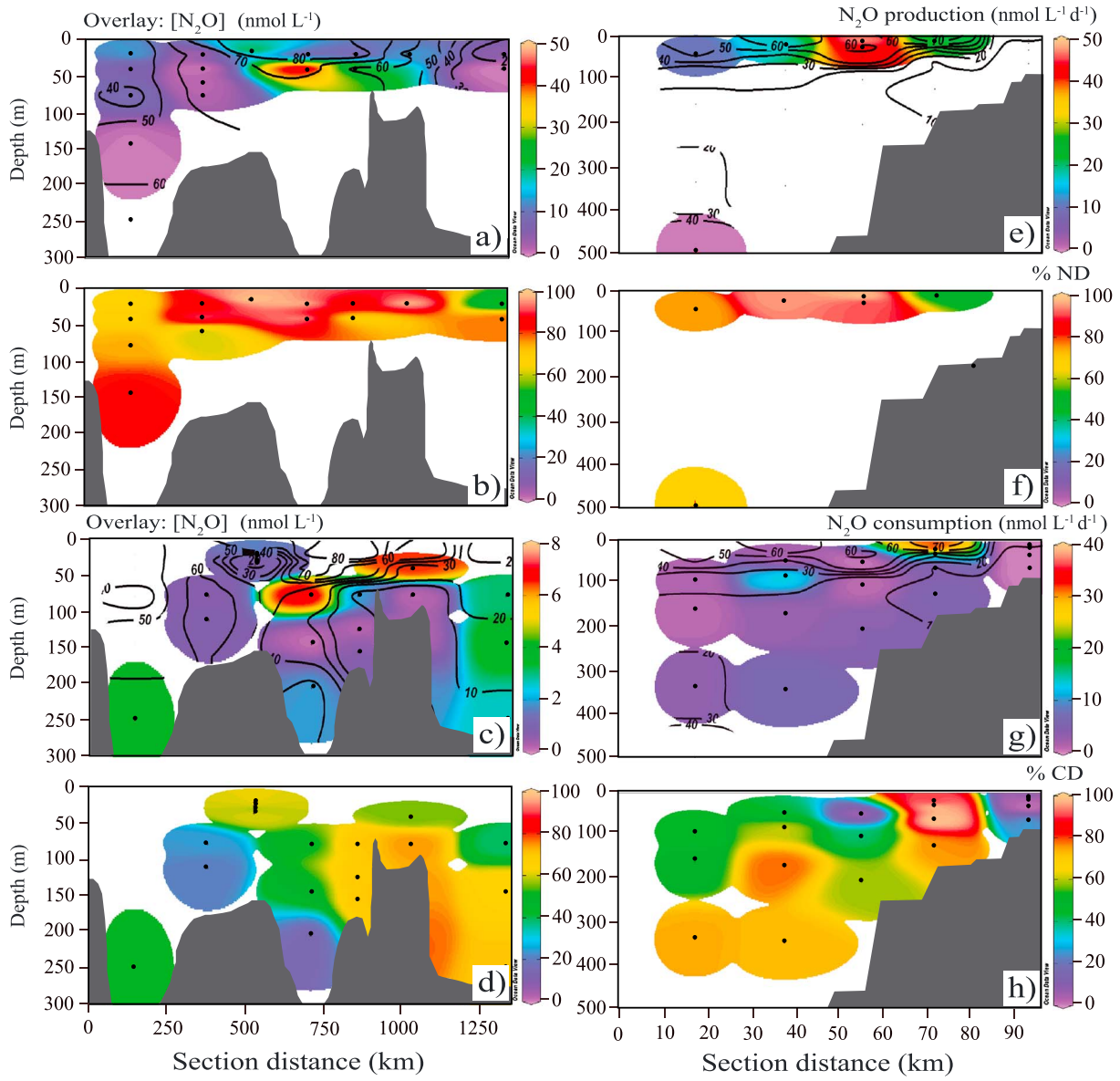

Figure 8. Results from the 3-D-reaction-advection-diffusion box models. Profiles of model (a and e) diagnosed rates of N_2O production in oxygenated waters ($[O_2] > 5\ \mu mol\ L^{-1}$) with N_2O concentrations in overlay, (b and f) diagnosed % N_2O produced from nitrifier-denitrification (ND) (or incomplete denitrifier-denitrification) relative to total N_2O production assuming a SP of 0‰ for nitrifier-denitrification and 34‰ for hydroxylamine oxidation, (c and g) diagnosed rates of N_2O consumption in the ODZ ($[O_2] < 5\ \mu mol\ L^{-1}$) with N_2O concentrations in overlay, and (d and h) diagnosed % N_2O consumption by denitrification (CD) relative to consumption assuming a SP of −0.5‰ for N_2O production by denitrification and an isotope effect of 16‰ during N_2O consumption along coastal transects A (Figures 8a–8d) and B (Figures 8e–8h). Individual data points represent the average value for each model box (see Figures S3 and S4). See Tables S1 to S3 for sensitivity of results to assuming different SP values and isotope effects.

Throughout the nondentrifying portions of our study area ($O_2 > 5\ \mu mol\ L^{-1}$), relatively low SPs (−3 to 26‰) were observed, with most values around ~ −3 to 14‰, especially for transect A (Figures 3, 4, and 6a, 6b). This and results from our box model (Figures 8b and 8f) suggest that nitrifier (or incomplete denitrifier)-denitrification is the dominant N_2O source.

Prior studies of Peru coastal waters note the occurrence of high ΔN_2O in oxic ($[O_2] > 5\ \mu mol\ L^{-1}$) near-surface waters (up to 1000 nmol L^{-1} [see *Arévalo-Martínez et al.*, 2015; *Kock et al.*, 2016]) (Figures 3d and 4d). In both transects A and B, highest ΔN_2O (up to 180 nmol L^{-1}) is found near surface at a number of stations (Figures 3 and 4). Though representing a minority of our samples, these patches of high N_2O are likely the most

important regional sources of N_2O to the atmosphere and their apparent isolation suggests N_2O production processes unique to them. These high N_2O accumulations likely resulted from a decoupling between N_2O production and consumption by denitrifiers as upwelling ODZ waters are partially re-oxygenated. The largest N_2O accumulations were all observed in the PCW water mass (Figure 5) [*Kock et al.*, 2016] associated with coastal upwelling. Such uncoupling of N_2O production and consumption as a consequence of varying O_2 has been attributed to incomplete denitrifier (or stop and go)-denitrification [*Naqvi et al.*, 2000; *Codispoti et al.*, 2001]. The threshold O_2 concentrations for N_2O production and consumption by denitrification are still not well known but appear to be higher for production. O_2 limits have been reported as high as 25 μmol L^{-1} for NO_3^- reduction [*Kalvelage et al.*, 2011] and 10 μmol L^{-1} for N_2O reduction to N_2 gas [*Zamora et al.*, 2012]. *Dalsgaard et al.* [2014] suggested an even lower [O_2] limit for N_2O consumption of 200 nmol L^{-1}, which is well below the detection limit of our Seabird O_2 sensor (~3 to 5 μmol L^{-1}).

Previously, highest N_2O accumulations have been observed in the coastal upwelling regions off major coastal ODZs, for instance in the Arabian Sea [*Naqvi et al.*, 2010] and in the ETSP off Peru and Chile [*Arévalo-Martínez et al.*, 2015; *Farías et al.*, 2015; *Kock et al.*, 2016], consistent with incomplete denitrifier-denitrification in near-surface waters as a likely important process in these regions. In addition to producing O_2 transients, coastal upwelling is also associated with high inputs of organic matter and cryptic H_2S cycling [see *Canfield et al.*, 2010], which are substrates during heterotrophic and autotrophic denitrification and can thus also contribute to ΔN_2O accumulation [e.g., *Babbin et al.*, 2014; *Dalsgaard et al.*, 2014]. Overall, organic matter export and denitrification are particularly enhanced in high productivity shelf regions of ODZ's [e.g., *Kalvelage et al.*, 2013; *Babbin et al.*, 2014].

Given low SP values, the only alternative to incomplete denitrifier-denitrification for these high N_2O accumulations would be nitrifier-denitrification. If we assume that nitrifier-denitrification is coupled to aerobic organic matter remineralization, a relationship between AOU and ΔN_2O should be observed as reported for offshore waters off Peru [*Ryabenko et al.*, 2012; *Kock et al.*, 2016] and other marine ODZs [*Cohen and Gordon*, 1978; *De Wilde and Helder*, 1997; *Upstill-Goddard et al.*, 1999]. Such a relationship was not observed in coastal waters off Peru [*Kock et al.*, 2016; this study]. Instead, the extreme ΔN_2O observed in shelf surface waters were generally associated with the strongest deviations from the ΔN_2O/AOU ratio observed offshore and highest N loss, suggesting that N_2O accumulation likely occurred after re-oxygenation of waters upwelled from the ODZ [*Kock et al.*, 2016]. ^{15}N-labeled incubation experiments by *Ji et al.* [2015] also showed that denitrifier-denitrification was the major N_2O production pathway responsible for at least 50% of total N_2O production just above the ODZ in the ETSP. However, nitrifier-denitrification could be decoupled from aerobic organic matter remineralization if it is fueled by NO_2^- produced from NO_3^- reduction in the ODZ.

While it is not possible to distinguish between N_2O production by nitrifier-denitrification coupled to aerobic remineralization or denitrifier- denitrification from their isotopomer signatures alone because of their similar low SP (Table 1), our isotopic data do show strong coupling between NO_3^- and NO_2^- with N_2O in these patches of very high N_2O concentrations. Significant relationships were observed between δ^{15}N-NO_3^-, and δ^{15}N-N_2O at O_2 concentrations between 5 μmol L^{-1} and 50 μmol L^{-1} at or above the oxycline (Figures 7a and 7b). In particular, highly significant relationships were also observed between δ^{18}O-NO_3^- and δ^{18}O-N_2O for the same O_2 range (Figures 7c and 7d). As NO_3^- is a substrate for N_2O production during denitrification, but not nitrifier-denitrification coupled to aerobic organic matter remineralization, these relationships indicate that high N_2O in near-surface waters likely originated from partly denitrified NO_3^- upwelled from the ODZ. In contrast, a relationship between δ^{15}N-NO_2^-, a substrate during both nitrifier-denitrification and denitrification, and δ^{15}N-N_2O was only observed for transect B at O_2 concentrations between 5 μmol L^{-1} and 50 μmol L^{-1} (Figures 7e and 7f).

No such relationships were observed for $O_2 > 50$ μmol L^{-1}. Phytoplankton NO_3^- assimilation and associated fractionation in oxygenated surface waters would likely erase any relationship between NO_3^- and N_2O isotopes. However, the high δ^{18}O-N_2O (up to 70‰) associated with high N_2O concentrations observed at [O_2] > 50 μmol L^{-1} (Figures 3 and 4) suggests that N_2O likely originated from partly denitrified NO_3^- enriched in ^{18}O and was produced at lower O_2 concentrations near the oxycline before being upwelled to the surface. Overall, our results suggest that incomplete denitrifier-denitrification or nitrifier-denitrification fueled by NO_2^- from upwelled ODZ waters are likely pathways for the extreme N_2O accumulation in surface waters off the Peru coast. As N_2O produced in aged source waters is largely consumed in the ODZ (see section 4.2),

these N_2O production mechanisms might represent the major way by which these regions contribute to the ocean's N_2O flux to the atmosphere.

Assuming a total area of 2.22×10^5 km^2 for the Peruvian upwelling (as in *Arévalo-Martínez et al.* [2015]), a 10 m layer above the ODZ where N_2O production exceed consumption ($5\ \mu mol\ L^{-1} > [O_2] < 25\ \mu mol\ L^{-1}$; from our data and *Babbin et al.* [2015]) and a N_2O production rate of up to 49 nmol $N_2O\ L^{-1}\ d^{-1}$ in this layer (Figures 8a and 8e), we obtain an efflux of up to 1.75 Tg $N_2O\ yr^{-1}$ (0.6 Tg N yr^{-1}). Our estimate is similar to the massive efflux of 0.2–0.9 Tg N yr^{-1} (5 to 22% of previous estimates of global marine N_2O emissions) independently inferred from high-resolution surface measurements and gas exchange parameterizations during the same research expeditions by *Arévalo-Martínez et al.* [2015]. The distinct isotopic signature of marine N_2O produced by incomplete denitrifier-denitrification or nitrifier-denitrification fueled by NO_2^- supplied from the ODZ could significantly modify the average atmospheric N_2O isotope and isotopomer composition from river, estuary, and coastal areas over time ($\delta^{15}N^{bulk} = -1.3$ ‰, $\delta^{18}O = 39.1$‰, and SP = 23.3‰ [*Toyoda et al.*, 2013]), as we generally observed lower SPs and higher $\delta^{18}O$ in surface waters (Figures 7a and 7b).

4.2. N_2O Consumption and Production by Denitrification in the ODZ

As illustrated in Figures 3 and 4, once O_2 is $<5\ \mu mol\ L^{-1}$, N-loss process including denitrification is activated leading to an accumulation of biogenic N_2 and loss of N_2O as well as an accumulation of NO_2^- and isotopic enrichment of both NO_3^- and NO_2^- (Figure S5). Thus, much if not most of the N_2O accumulated in aging intermediate waters can be consumed by reduction to N_2 if these waters "terminate" in an ODZ. In this sense, ODZ's could act to reduce the oceanic flux of N_2O to the atmosphere. Assuming an area of 2.22×10^5 km^2 for the Peruvian upwelling, a maximum layer of 300 m for the ODZ ($O_2 < 5\ \mu mol\ L^{-1}$; this study) and a maximum N_2O consumption rate of 38 nmol $N_2O\ L^{-1}\ d^{-1}$ (Figure 8g), up to 41 Tg $N_2O\ yr^{-1}$ (13 Tg N yr^{-1}), could be removed in coastal waters off Peru, which is about 23 times the maximum efflux calculated in this study. In fact, the ODZ layer is generally less than 300 m in coastal areas (see Figures 3 and 4) and N_2O consumption rate generally 1 order of magnitude smaller (see Figures 8c and 8g). This estimate thus represents an absolute upper limit on N_2O loss from the coastal ODZ off Peru.

The isotopomer signals associated with net N_2O consumption are clearly seen in our study region for samples with $O_2 < 5\ \mu mol\ L^{-1}$. N_2O consumption leads to an increase in SP and $\delta^{18}O$ as observed in both transects (Figures 3, 4, and 6). The slopes of the relationships for SP versus $\delta^{18}O$-N_2O were, however, generally greater than the value of 1:2.2 expected for pure N_2O consumption at both transects [*Ostrom et al.*, 2007] (Figures 6a and 6b). Deviation from a slope of 1:2.2 (0.455) for pure N_2O consumption was also observed by *Frame et al.* [2014] for water impacted by denitrification in the South Atlantic and was attributed to mixing and long-range horizontal transport.

As noted above, while $\delta^{15}N^{\alpha}$ increased with $\delta^{18}O$ in the ODZ, $\delta^{15}N^{\beta}$ generally remained the same or decreased (Figures 6e and 6f). It follows that most of the increase in SP with increasing $\delta^{18}O$ is due to ^{15}N enrichment in the α N atom. A similar trend was also observed at offshore stations in December 2012 (data not shown). From a mechanistic perspective, this is expected as the consumption of N_2O by denitrification involves just the breaking of the bond between the α-position N and O to produce N_2 (Figure 1). This observation, though, is only in partial agreement with laboratory observations in which $\delta^{15}N^{\alpha}$ and $\delta^{15}N^{\beta}$ both increase during N_2O consumption by denitrification but the latter to a lesser degree [*Jinuntuya-Nortman et al.*, 2008; *Ostrom et al.*, 2007; *Yamagishi et al.*, 2007] (Table 1). Such a decrease in $\delta^{15}N^{\beta}$ accompanied with increases in $\delta^{15}N^{\alpha}$, $\delta^{18}O$, and SP was also previously observed in low-O_2 waters ($<5\ \mu mol\ L^{-1}$) of the ETNP [*Yamagishi et al.*, 2007] and the Black Sea [*Westley et al.*, 2006] and attributed to shifts from N_2O consumption to net production. N_2O production by denitrification (like the nitrifier-denitrifier pathway) is associated with a low SP of ~0‰ [*Sutka et al.*, 2006] and is thus expected to add almost equally low $\delta^{15}N^{\alpha}$-N_2O and $\delta^{15}N^{\beta}$-N_2O. A shift from N_2O consumption to net production could thus offset the effect of N_2O consumption for $\delta^{15}N^{\beta}$-N_2O and cause it to decrease relative to $\delta^{15}N^{\alpha}$-N_2O.

While net N_2O consumption is observed in the coastal Peru ODZ, denitrifying bacteria must also be producing N_2O (Figure 1) which may exchange with the external pool. In support, *Babbin et al.* [2015] found that N_2O production mostly balanced consumption in the offshore ETNP ODZ based on N_2O reduction rates from tracer incubations and a 1-D model. N_2O concentration profiles at these offshore stations were hence

relatively unchanged over time despite a fast N_2O turnover. In more dynamic coastal ODZ's such as in this study, we observed heterogeneous imbalance between production and consumption from our box model, which is expected as N turnover is generally faster [*Hu et al.*, 2016] and N_2O concentrations in the water column are more spatially and temporally variable [*Kock et al.*, 2016; this study].

Concurrent N_2O production in the ODZ should be evident in coupling of the isotopic signature of N_2O with the signatures of precursor NO_3^- and NO_2^-. NO_3^- and NO_2^- increase dramatically in $\delta^{15}N$ and $\delta^{18}O$ with increasing N loss (Figure S5) following kinetic isotope fractionation. Indeed, significant positive correlations between $\delta^{15}N^{bulk}$-NO_3^- and $\delta^{15}N$-NO_3^- as well as $\delta^{15}N$-NO_2^- were observed for samples with $O_2 < 5\ \mu mol\ L^{-1}$ for both transects A and B (Figure 7). However, slopes were significantly less than 1 likely indicating other processes simultaneously affecting the substrate and product pools. For instance, NO_2^- oxidation to NO_3^- is associated with an inverse ^{15}N kinetic isotope effect of −13‰ (*Casciotti*, 2009) and thus raises the $\delta^{15}N$-NO_3^- and lowers the $\delta^{15}N$-NO_2^-. Similarly, N_2O consumption enhances $\delta^{15}N$-N_2O as discussed earlier. Different degrees of NO_2^- re-oxidation and N_2O consumption at non-steady state conditions could thus cause the $\delta^{15}N$-N_2O/$\delta^{15}N$-NO_3^- and $\delta^{15}N$-N_2O/$\delta^{15}N$-NO_2^- slopes to deviate from 1. It is, however, not clear why, for the same sample set, $\delta^{18}O$-N_2O and $\delta^{18}O$-NO_3^- appeared to be positively correlated only at low $\delta^{18}O$-NO_3^- values. In addition to kinetic isotope effects [see *Frame and Casciotti*, 2010], $\delta^{18}O$ of N_2O is impacted by branching isotope effects during NO_3^- and NO_2^- reduction to N_2O, that elevate the $\delta^{18}O$ of N_2O relative to its $\delta^{15}N$ [*Casciotti et al.*, 2007]. The NO_2^- oxygen atoms also tend to slowly equilibrate with water on a time scale of weeks to months, depending on in situ temperature and pH, with a $\delta^{18}O$ of ~14‰ at equilibrium [*Buchwald and Casciotti*, 2013]. As NO_2^- turnover in the coastal ODZ off Peru is relatively fast [*Hu et al.*, 2016], its $\delta^{18}O$ likely would not have sufficient time to fully equilibrate with H_2O (see Figures S5c and S5d). However, even partial ^{18}O equilibration with water could decrease the $\delta^{18}O$ of NO_2^- and add a relatively low $\delta^{18}O$ to the N_2O pool following NO_2^- reduction, affecting the relationship between $\delta^{18}O$-N_2O and $\delta^{18}O$-NO_3^- (Figures 7c and 7d) and potentially increasing the slope for SP versus $\delta^{18}O$-N_2O (see Figure 6a, transect A, where slope near 1 was observed). This was especially observed where NO_2^- significantly accumulated, and where NO_3^- was depleted and $\delta^{18}O$-NO_3^- high.

Our data also supported gross N_2O production even at the highest extent of N loss. Low SPs were observed where NO_3^- and NO_2^- were almost completely consumed and biogenic N_2 was the highest in the ODZ at the shallowest stations 63 (transect A) and 9 (transect B) (Figure 6). At these stations, both $\delta^{15}N^{\alpha}$-N_2O and $\delta^{15}N^{\beta}$-N_2O were elevated and closer to the isotopic composition of the substrates (NO_3^- and NO_2^-) when present. ΔN_2O was also slightly above 0, i.e., equilibrium, at station 63, transect A (8 nmol L^{-1}) and station 9, transect B (up to 11.5 nmol L^{-1}). As SP is not affected by the initial isotopic composition of the substrate nor fractionated during N_2O production [*Sutka et al.*, 2006], the observed low SPs, along with N_2O concentrations above equilibrium, suggest N_2O production in the ODZ at these shallow stations, in accordance with our model (Figure 8h). Organic matter, a substrate for denitrification (and hence N_2O production), decreases exponentially with depth below the euphotic zone [*Martin et al.*, 1987], potentially explaining the higher relative N_2O production (versus consumption) at these shallow stations.

For completeness, abiotic N_2O production by iron reduction of NO_2^- needs to be considered as a source of N_2O in the ODZ. Reduced iron as well as NO_2^- is present in the ODZ, making this reaction possible although there is currently no evidence for significant reaction rates. High SPs (30–36‰ [e.g., *Toyoda et al.*, 2005; *Heil et al.*, 2014]) are typically associated with abiotic N_2O production by various pathways involving the nitrification intermediates hydroxylamine or NO_2^- in combination with iron compounds or other transition metals. However, accounting for abiotic N_2O production in our box models suggested that this process did not significantly contribute to our observations, with the SP signature of N_2O production from metal reduction failing to predict the observed SP in most boxes for the computed mixing rates.

5. Summary and Concluding Remarks

We observed extreme N_2O concentrations of up to 190 nmol L^{-1} in surface waters off the Peru coast during December 2012 and January 2013, as previously reported by *Arévalo-Martínez et al.* [2015] and *Kock et al.* [2016].

We consistently observed low SPs in surface waters above the oxycline, mostly ranging from −3 to 14‰. Our model diagnosed biological fluxes suggested that nitrifier-denitrification or incomplete denitrifier-denitrification generally represented more than 50% of total N_2O production. While N_2O production by nitrifier-denitrification and denitrifier-denitrification have similar SP, making it impossible to distinguish between these two processes, several lines of evidence suggested that incomplete denitrifier-denitrification as waters are upwelled from the ODZ and re-oxygenated or nitrifier-denitrification fueled by NO_2^- from NO_3^- reduction in the ODZ are likely pathways for N_2O production in surface waters. Main indications were as follows: (1) the highest N_2O accumulations were observed in the PCW water mass, which is associated with upwelling; (2) there was no relationship between ΔN_2O and AOU as expected for N_2O production by nitrification coupled to aerobic organic matter remineralization; and (3) we observed significant relationships between $\delta^{15}N_{bulk}$-N_2O and $\delta^{15}N$ and $\delta^{18}O$ of NO_3^-, a substrate for N_2O production during denitrification, above the oxycline. We estimated an efflux of up to 0.6 Tg N yr^{-1} from nitrifier or incomplete denitrifier-denitrification, which is comparable to the estimate by *Arévalo-Martínez et al.* [2015].

We further used 3-D-reaction-advection-diffusion regional box models to investigate the rates and modes of N_2O production in surface waters and the rates of production and consumption in the ODZ. We estimated that a maximum of 13 Tg N yr^{-1} could be removed in the coastal ODZ off Peru, which was about 23 times the maximum N_2O efflux. Our model diagnosed fluxes showed a decoupling between N_2O production and consumption, with generally higher relative N_2O consumption as biogenic N_2 increased. A decrease or no change in $\delta^{15}N^{\beta}$-N_2O concomitant with increasing $\delta^{15}N^{\alpha}$-, $\delta^{18}O$-N_2O, and SP was generally observed in the ODZ. At the shallowest stations, at near substrate consumption, where the $\delta^{15}N$ of NO_2^- and NO_3^- were also the highest, we observed high values for both $\delta^{15}N^{\beta}$-N_2O and $\delta^{15}N^{\alpha}$-N_2O, generally associated with low SPs. N_2O concentrations were also close or above equilibrium values at these stations. These observations likely indicated shifts from N_2O consumption to N_2O production in the ODZ, even at the highest extent of N loss.

Overall, our results show a strong spatial heterogeneity in the mechanisms controlling N_2O production and consumption in shallow waters off Peru, which should be better taken into account in global oceanic N_2O models.

Acknowledgments

Data for this paper are available on the Data Management Portal for Kiel Marine Sciences hosted at GEOMAR (M91 and M92 cruises): https://portal.geomar.de/. This work was supported by the Deutsche Forschungsgemeinschaft project SFB-754 (www.sfb754.de), SOPRANII (grant FKZ03F0611A; www.sopran.pangaea.de), and a NSERC Postdoctoral Fellowship to A.B. R.T.L. was supported by DOE Office of Science grant DE-SC0016329. We would like to thank the captain and crew of R/V *Meteor* during the M91 and M92 cruises and Daniel Kiefhaber, Avi Bernales and Violeta Leon for their help during sampling. We thank the authorities of Peru for the permission to work in their territorial waters. The modeling part of the study has been conducted by using the Copernicus Marine Service Products.

References

Altabet, M. A. (2001), Nitrogen isotopic evidence for micronutrient control of fractional NO_3^- utilization in the equatorial Pacific, *Limnol. Oceanogr.*, *46*(2), 368–380.

Altabet, M. A. (2006), Isotopic tracers of the marine nitrogen cycle: Present and past, in *Marine Organic Matter: Chemical and Biological Markers, Isotopes and DNA, The Handbook of Environmental Chemistry*, vol. 2N, edited by J. K. Volkman, chap. 8, pp. 251–293, Springer, Berlin.

Arévalo-Martínez, D. L., A. Kock, C. R. Löscher, R. A. Schmitz, and H. W. Bange (2015), Massive nitrous oxide emissions from the tropical South Pacific Ocean, *Nat. Geosci.*, *8*(7), 530–533.

Babbin, A. R., R. G. Keil, A. H. Devol, and B. B. Ward (2014), Organic matter stoichiometry, flux, and oxygen control nitrogen loss in the ocean, *Science*, *344*, 406–408.

Babbin, A. R., D. Bianchi, A. Jayakumar, and B. B. Ward (2015), Rapid nitrous oxide cycling in the suboxic ocean, *Science*, *348*(6239), 1127–1129.

Bange, H. W., S. Rapsomanikis, and M. O. Andreae (2001), Nitrous oxide cycling in the Arabian Sea, *J. Geophys. Res.*, *106*(C1), 1053–1065, doi:10.1029/1999JC000284.

Barford, C. C., J. P. Montoya, M. A. Altabet, and R. Mitchell (1999), Steady-state nitrogen isotope effects of N_2 and N_2O production in *Paracoccus denitrificans*, *Environ. Microbiol.*, *65*, 989–994.

Barnier, B., L. Siefridt, and P. Marchesiello (1995), Thermal forcing for a global ocean circulation model using a three-year climatology of ECMWF analyses, *J. Mar. Syst.*, *6*, 363–380.

Bourbonnais, A., M. F. Lehmann, J. J. Waniek, and D. E. Schulz-Bull (2009), Nitrate isotope anomalies reflect N_2 fixation in the Azores Front region (subtropical NE Atlantic), *J. Geophys. Res.*, *114*, C03003, doi:10.1029/2007JC004617.

Bourbonnais, A., M. A. Altabet, C. N. Charoenpong, J. Larkum, H. Hu, H. W. Bange, and L. Stramma (2015), N-loss isotope effects in the Peru oxygen minimum zone studied using a mesoscale eddy as a natural tracer experiment, *Global Biogeochem. Cycles*, *29*, 793–811, doi:10.1002/2014GB005001.

Brandes, J. A., A. H. Devol, T. Yoshinari, D. A. Jayakumar, and S. W. A. Naqvi (1998), Isotopic composition of nitrate in the central Arabian Sea and eastern tropical North Pacific: A tracer for mixing and nitrogen cycles, *Limnol. Oceanogr.*, *43*(7), 1680–1689.

Brunner, B., et al. (2013), Nitrogen isotope effects induced by anammox bacteria, *Proc. Natl. Acad. Sci. U.S.A.*, *110*(47), 18,994–18,999.

Bryan, B. A., G. Shearer, J. L. Skeeters, and D. H. Kohl (1983), Variable expression of the nitrogen isotope effect associated with denitrification of nitrite, *J. Biol. Chem.*, *258*, 8613–8617.

Buchwald, C., and K. L. Casciotti (2013), Isotopic ratios of nitrite as tracers of the sources and age of oceanic nitrite, *Nat. Geosci.*, *6*(4), 308–313.

Canfield, D. E., F. J. Stewart, B. Thamdrup, L. De Brabandere, T. Dalsgaard, E. F. Delong, N. P. Revsbech, and O. Ulloa (2010), A cryptic sulfur cycle in oxygen-minimum-zone waters off the Chilean coast, *Science*, *330*(6009), 1375–1378.

Casciotti, K. L. (2009), Inverse kinetic isotope fractionation during bacterial nitrite oxidation, *Geochim. Cosmochim. Acta*, *73*(7), 2061–2076.
Casciotti, K. L., and M. R. McIlvin (2007), Isotopic analyses of nitrate and nitrite from reference mixtures and application to Eastern Tropical North Pacific waters, *Mar. Chem.*, *107*(2), 184–201.
Casciotti, K. L., D. M. Sigman, M. G. Hastings, J. K. Böhlke, and A. Hilkert (2002), Measurement of the oxygen isotopic composition of nitrate in seawater and freshwater using the denitrifier method, *Anal. Chem.*, *74*(19), 4905–4912.
Casciotti, K. L., J. K. Böhlke, M. R. McIlvin, S. J. Mroczkowski, and J. E. Hannon (2007), Oxygen isotopes in nitrite: Analysis, calibration, and equilibration, *Anal. Chem.*, *79*(6), 2427–2436, doi:10.1021/ac061598h.
Charoenpong, C. N., L. A. Bristow, and M. A. Altabet (2014), A continuous flow isotope ratio mass spectrometry method for high precision determination of dissolved gas ratios and isotopic composition, *Limnol. Oceanogr. Methods*, *12*, 323–337.
Ciais, P., et al. (2013), Carbon and other biogeochemical cycles, in *Climate Change 2013: The Physical Science Basis. Contribution of Working Group I to the Fifth Assessment Report of the Intergovernmental Panel on Climate Change*, edited by T. F. Stocker et al., Cambridge Univ. Press, Cambridge, U. K., and New York.
Codispoti, L. A., J. A. Brandes, J. P. Christensen, A. H. Devol, S. W. A. Naqvi, H. W. Paerl, and T. Yoshinari (2001), The oceanic fixed nitrogen and nitrous oxide budgets: Moving targets as we enter the anthropocene?, *Sci. Mar.*, *65*, 85–105.
Cohen, Y., and L. I. Gordon (1978), Nitrous oxide in the oxygen minimum of the eastern tropical North Pacific: Evidence for its consumption during denitrification and possible mechanisms for its production, *Deep Sea Res.*, *25*, 509–524.
Cohen, Y., and L. I. Gordon (1979), Nitrous oxide production in the Ocean, *J. Geophys. Res.*, *84*(C1), 347–353, doi:10.1029/JC084iC01p00347.
Da Silva, A. M., C. C. Young, and S. Levitus (1994), Atlas of surface marine data 1994, vol. 1, Algorithms and procedures, technical report, Natl. Oceanogr. and Atmos. Admin., Silver, Spring, Md.
Dalsgaard, T., F. J. Stewart, B. Thamdrup, L. De Brabandere, N. P. Revsbech, O. Ulloa, D. E. Canfield, and E. F. DeLong (2014), Oxygen at nanomolar levels reversibly suppresses process rates and gene expression in anammox and denitrification in the oxygen minimum zone off northern Chile, *MBio*, *5*(6), e01966–14, doi:10.1128/mBio.01966-14.
De Wilde, H. P. J., and W. Helder (1997), Nitrous oxide in the Somali Basin: The role of upwelling, *Deep Sea Res., Part II*, *44*(6–7), 1319–1340.
Echevin, V., F. Colas, A. Chaigneau, and P. Penven (2011), Sensitivity of the Northern Humboldt Current System nearshore modeled circulation to initial and boundary conditions, *J. Geophys. Res.*, *116*, C07002, doi:10.1029/2010JC006684.
Farías, L., V. Besoain, and S. García-Loyola (2015), Presence of nitrous oxide hotspots in the coastal upwelling area off central Chile: An analysis of temporal variability based on ten years of a biogeochemical time series, *Environ. Res. Lett.*, *10*(4), 1–13, doi:10.1088/1748-9326/10/4/044017.
Forster, P., et al. (2007), Changes in atmospheric constituents and in radiative forcing, in *Climate Change 2007: The Physical Science Basis. Contribution of Working Group I to the Fourth Assessment Report of the Intergovernmental Panel on Climate Change*, edited by S. Solomon et al., Cambridge Univ. Press, Cambridge, U. K., and New York.
Frame, C. H., and K. L. Casciotti (2010), Biogeochemical controls and isotopic signatures of nitrous oxide production by a marine ammonia-oxidizing bacterium, *Biogeosciences*, *7*(9), 2695–2709.
Frame, C. H., E. Deal, C. D. Nevison, and K. L. Casciotti (2014), N_2O production in the eastern South Atlantic: Analysis of N_2O stable isotopic and concentration data, *Global Biogeochem. Cycles*, *28*, 1262–1278, doi:10.1002/2013GB004790.
Freing, A., D. W. R. Wallace, and H. W. Bange (2012), Global oceanic production of nitrous oxide, *Philos. Trans. R. Soc. B.: Biol. Sci.*, *367*(1593), 1245–1255.
Goreau, T. J., W. A. Kaplan, S. C. Wofsy, M. B. McElroy, F. W. Valois, and S. W. Watson (1980), Production of NO_2^- and N_2O by nitrifying bacteria at reduced concentrations of oxygen, *Appl. Environ. Microbiol.*, *40*(3), 526–532.
Granger, J., and D. M. Sigman (2009), Removal of nitrite with sulfamic acid for nitrate N and O isotope analysis with the denitrifier method, *Rapid Commun. Mass Spectrom.*, *23*(23), 3753–3762.
Granger, J., D. M. Sigman, J. A. Needoba, and P. J. Harrison (2004), Coupled nitrogen and oxygen isotope fractionation of nitrate during assimilation by cultures of marine phytoplankton, *Limnol. Oceanogr.*, *49*(5), 1763–1773.
Granger, J., D. M. Sigman, M. F. Lehmann, and P. D. Tortell (2008), Nitrogen and oxygen isotope fractionation during dissimilatory nitrate reduction by denitrifying bacteria, *Limnol. Oceanogr.*, *53*(6), 2533–2545.
Hamme, R. C., and S. R. Emerson (2002), Mechanisms controlling the global oceanic distribution of the inert gases argon, nitrogen and neon, *Geophys. Res. Lett.*, *29*(23), 2120, doi:10.1029/2002GL015273.
Heil, J., B. Wolf, N. Brüggemann, L. Emmenegger, B. Tuzson, H. Vereecken, and J. Mohn (2014), Site-specific ^{15}N isotopic signatures of abiotically produced N_2O, *Geochim. Cosmochim. Acta*, *139*(C), 72–82.
Hu, H., A. Bourbonnais, J. Larkum, H. W. Bange, and M. A. Altabet (2016), Nitrogen cycling in shallow low-oxygen coastal waters off Peru from nitrite and nitrate nitrogen and oxygen isotopes, *Biogeosciences*, *13*(5), 1453–1468, doi:10.5194/bg-13-1453-2016.
Ji, Q., A. R. Babbin, A. Jayakumar, S. Oleynik, and B. B. Ward (2015), Nitrous oxide production by nitrification and denitrification in the Eastern Tropical South Pacific oxygen minimum zone, *Geophys. Res. Lett.*, *42*, 10,755–10,764, doi:10.1002/2015GL066853.
Jinuntuya-Nortman, M., R. L. Sutka, P. H. Ostrom, H. Gandhi, and N. E. Ostrom (2008), Isotopologue fractionation during microbial reduction of N_2O within soil mesocosms as a function of water-filled pore space, *Soil Biol. Biochem.*, *40*, 2273–2280, doi:10.1016/j.soilbio.20.
Kalvelage, T., M. M. Jensen, S. Contreras, N. P. Revsbech, P. Lam, M. Günter, J. LaRoche, G. Lavik, and M. M. M. Kuypers (2011), Oxygen sensitivity of anammox and coupled N-cycle processes in oxygen minimum zones, edited by J. A. Gilbert, *PLoS One*, *6*(12), e29299, doi:10.1371/journal.pone.0029299.t003.
Kalvelage, T., G. Lavik, P. Lam, S. Contreras, L. Arteaga, C. R. Löscher, A. Oschlies, A. Paulmier, L. Stramma, and M. M. M. Kuypers (2013), Nitrogen cycling driven by organic matter export in the South Pacific oxygen minimum zone, *Nat. Geosci.*, *6*(3), 228–234.
Kock, A., D. L. Arévalo-Martínez, C. R. Löscher, and H. W. Bange (2016), Differences between coastal and open ocean distributions of N_2O in the oxygen minimum zone off Peru, *Biogeosciences*, *13*, 827–840.
Kool, D. M., J. W. Van Groenigen, and N. Wrage (2011), Source determination of nitrous oxide based on nitrogen and oxygen isotope tracing: Dealing with oxygen exchange, in *Methods in Enzymology*, vol. 496, edited by M. G. Klotz and L. Y. Stein, pp. 139–160, Academic Press, Burlington.
Law, C. S., and N. J. P. Owens (1990), Significant flux of atmospheric nitrous oxide from the northwest Indian Ocean, *Nature*, *346*, 826–828.
Lewicka-Szczebak, D., R. Well, R. Bol, A. S. Gregory, G. P. Matthews, T. Misselbrook, W. R. Whalley, and L. M. Cardenas (2015), Isotope fractionation factors controlling isotopocule signatures of soil-emitted N_2O produced by denitrification processes of various rates, *Rapid Commun. Mass Spectrom.*, *29*, 269–282.
Löscher, C. R., A. Kock, M. Könneke, J. LaRoche, H. W. Bange, and R. A. Schmitz (2012), Production of oceanic nitrous oxide by ammonia-oxidizing archaea, *Biogeosciences*, *9*(7), 2419–2429.

Mandernack, K. W., T. Rahn, C. Kinney, and M. Wahlen (2000), The biogeochemical controls of the $\delta^{15}N$ and $\delta^{18}O$ of N_2O produced in landfill cover soils, *J. Geophys. Res.*, *105*(D14), 17,709–720, doi:10.1029/2000JD900055.

Martin, J. H., G. A. Knauer, D. M. Karl, and W. W. Broenkow (1987), VERTEX: Carbon cycling in the northeast Pacific, *Deep Sea Res. Part A*, *34*, 267–285.

McIlvin, M. R., and K. L. Casciotti (2010), Fully automated system for stable isotopic analyses of dissolved nitrous oxide at natural abundance levels, *Limnol. Oceanogr. Methods*, *8*, 54–66.

McIlvin, M. R., and M. A. Altabet (2005), Chemical conversion of nitrate and nitrite to nitrous oxide for nitrogen and oxygen isotopic analysis in freshwater and seawater, *Anal. Chem.*, *77*(17), 5589–5595.

Menyailo, O. V., and B. A. Hungate (2006), Stable isotope discrimination during soil denitrification: Production and consumption of nitrous oxide, *Global Biogeochem. Cycles*, *20*, GB3025, doi:10.1029/2005GB002527.

Mohn, J., et al. (2014), Inter-laboratory assessment of nitrous oxide isotopomer analysis by isotope ratio mass spectrometry and laser spectroscopy: Current status and perspectives, *Rapid Commun. Mass Spectrom.*, *28*(18), 1995–2007.

Montes, I., W. Schneider, F. Colas, B. Blanke, and V. Echevin (2011), Subsurface connections in the eastern tropical Pacific during La Niña 1999–2001 and El Niño 2002–2003, *J. Geophys. Res.*, *116*, C12022, doi:10.1029/2011JC007624.

Naqvi, S. W. A., D. A. Jayakumar, P. V. Narvekar, H. Naik, V. V. S. S. Sarma, W. D'Souza, S. Joseph, and M. D. George (2000), Increased marine production of N_2O due to intensifying anoxia on the Indian continental shelf, *Nature*, *408*, 346–349.

Naqvi, S. W. A., H. W. Bange, L. Farías, P. M. S. Monteiro, M. I. Scranton, and J. Zhang (2010), Marine hypoxia/anoxia as a source of CH_4 and N_2O, *Biogeosciences*, *7*(7), 2159–2190.

Nevison, C. D., and E. Holland (1997), A reexamination of the impact of anthropogenically fixed nitrogen on atmospheric N_2O and the stratospheric O_2 layer, *J. Geophys. Res.*, *102*(D21), 25,519–25,536, doi:10.1029/97JD02391.

Nevison, C. D., R. F. Weiss, and D. J. Erickson III (1995), Global oceanic emissions of nitrous oxide, *J. Geophys. Res.*, *100*(C8), 15,809–15,820, doi:10.1029/95JC00684.

Nevison, C. D., T. J. Lueker, and R. F. Weiss (2004), Quantifying the nitrous oxide source from coastal upwelling, *Global Biogeochem. Cycles*, *18*, GB1018, doi:10.1029/2003GB002110.

Nevison, C., J. H. Butler, and J. W. Elkins (2003), Global distribution of N_2O and the ΔN_2O-AOU yield in the subsurface ocean, *Global Biogeochem. Cycles*, *17*(4), 1119, doi:10.1029/2003GB002068.

Ostrom, N. E., A. Pitt, R. Sutka, P. H. Ostrom, A. S. Grandy, K. M. Huizinga, and G. P. Robertson (2007), Isotopologue effects during N_2O reduction in soils and in pure cultures of denitrifiers, *J. Geophys. Res.*, *112*, G02005, doi:10.1029/2006JG000287.

Ostrom, N., and P. Ostrom (2011), The isotopomers of nitrous oxide: analytical considerations and application to resolution of microbial production pathways, in *Handbook of Environmental Isotope Geochemistry – Advances in Isotope Geochemistry*, Part 1, edited by M. Baskaran, pp. 453–476, Springer, Berlin.

Penven, P., V. Echevin, J. Pasapera, F. Colas, and J. Tam (2005), Average circulation, seasonal cycle, and mesoscale dynamics of the Peru Current System: A modeling approach, *J. Geophys. Res.*, *110*, C10021, doi:10.1029/2005JC002945.

Pietri, A., V. Echevin, P. Testor, A. Chaigneau, L. Mortier, C. Grados, and A. Albert (2014), Impact of a coastal-trapped wave on the near-coastal circulation of the Peru upwelling system from glider data, *J. Geophys. Res. Oceans*, *119*, 2109–2120, doi:10.1002/2013JC009270.

Ravishankara, A. R., J. S. Daniel, and R. W. Portmann (2009), Nitrous oxide (N_2O): The dominant ozone-depleting substance emitted in the 21st century, *Science*, *326*(5949), 123–125.

Ryabenko, E., A. Kock, H. W. Bange, M. A. Altabet, and D. W. R. Wallace (2012), Contrasting biogeochemistry of nitrogen in the Atlantic and Pacific oxygen minimum xones, *Biogeosciences*, *9*(1), 203–215.

Santoro, A. E., K. L. Casciotti, and C. A. Francis (2010), Activity, abundance and diversity of nitrifying archaea and bacteria in the central California Current, *Environ. Microbiol.*, *12*(7), 1989–2006.

Santoro, A. E., C. Buchwald, M. R. McIlvin, and K. L. Casciotti (2011), Isotopic signature of N_2O produced by marine ammonia-oxidizing Archaea, *Science*, *333*, 1282–1285.

Schmidt, H.-L., R. A. Werner, N. Yoshida, and R. Well (2004), Is the isotopic composition of nitrous oxide an indicator for its origin from nitrification or denitrification? A theoretical approach from referred data and microbiological and enzyme kinetic aspects, *Rapid Commun. Mass Spectrom.*, *18*(18), 2036–2040.

Shchepetkin, A. F., and J. C. McWilliams (2005), The regional oceanic modeling system (ROMS): A split-explicit, free-surface, topography-following-coordinate oceanic model, *Ocean Model.*, *9*, 347–404.

Sigman, D. M., K. L. Casciotti, M. Andreani, C. Barford, M. Galanter, and J. K. Böhlke (2001), A bacterial method for the nitrogen isotopic analysis of nitrate in seawater and freshwater, *Anal. Chem.*, *73*(17), 4145–4153.

Sigman, D. M., J. Granger, P. J. DiFiore, M. M. Lehmann, R. Ho, G. Cane, and A. van Geen (2005), Coupled nitrogen and oxygen isotope measurements of nitrate along the eastern North Pacific margin, *Global Biogeochem. Cycles*, *19*, GB4022, doi:10.1029/2005GB002458.

Snider, D. M., J. J. Venkiteswaran, S. L. Schiff, and J. Spoelstra (2012), Deciphering the oxygen isotope composition of nitrous oxide produced by nitrification, *Glob. Chang. Biol.*, *18*, 356–370.

Stramma, L., H. W. Bange, R. Czeschel, A. Lorenzo, and M. Frank (2013), On the role of mesoscale eddies for the biological productivity and biogeochemistry in the eastern tropical Pacific Ocean off Peru, *Biogeosciences*, *10*, 7293–7306.

Strub, P. T., J. M. Mesías, V. Montecino, J. Rutillant, and S. Salinas (1998), Coastal ocean circulation off western south America, in *The Sea*, vol. 11, edited by A. R. Robinson and K. H. Brink, pp. 273–313, John Wiley, New York.

Sutka, R. L., N. E. Ostrom, P. H. Ostrom, H. Gandhi, and J. A. Breznak (2003), Nitrogen isotopomer site preference of N_2O produced by *Nitrosomonas europaea* and *Methylococcus capsulatus* Bath, *Rapid Commun. Mass Spectrom.*, *17*, 738–745.

Sutka, R. L., N. E. Ostrom, P. H. Ostrom, H. Gandhi, and J. A. Breznak (2004), Erratum: Nitrogen isotopomer site preference of N_2O produced by Nitrosomonas europaea and Methylococcus capsulatus Bath, *Rapid Commun. Mass Spectrom.*, *18*, 1411–1412.

Sutka, R. L., N. E. Ostrom, P. H. Ostrom, J. A. Breznak, H. Gandhi, A. J. Pitt, and F. Li (2006), Distinguishing nitrous oxide production from nitrification and denitrification on the basis of isotopomer abundances, *Appl. Environ. Microbiol.*, *72*(1), 638–644.

Toyoda, S., N. Yoshida, T. Miwa, Y. Matsui, H. Yamagishi, U. Tsunogai, Y. Nojiri, and N. Tsurushima (2002), Production mechanism and global budget of N2O inferred from its isotopomers in the western North Pacific, *Geophys. Res. Lett.*, *29*(3), 1037, doi:10.1029/2001GL014311.

Toyoda, S., H. Mutobe, H. Yamagishi, N. Yoshida, and Y. Tanji (2005), Fractionation of N_2O isotopomers during production by denitrifier, *Soil Biol. Biochem.*, *37*(8), 1535–1545.

Toyoda, S., N. Kuroki, N. Yoshida, K. Ishijima, Y. Tohjima, and T. Machida (2013), Decadal time series of tropospheric abundance of N_2O isotopomers and isotopologues in the Northern Hemisphere obtained by the long-term observation at Hateruma Island, Japan, *J. Geophys. Res. Atmos.*, *118*, 3369–3381, doi:10.1002/jgrd.50221.

Upstill-Goddard, R. C., J. Barnes, and N. J. P. Owens (1999), Nitrous oxide and methane during the 1994 SW monsoon in the Arabian Sea/northwestern Indian Ocean, *J. Geophys. Res.*, *104*(C12), 30,067–30,084, doi:10.1029/1999JC900232.

Voss, M., J. W. Dippner, and J. Montoya (2001), Nitrogen isotope patterns in the oxygen-deficient waters of the Eastern Tropical North Pacific Ocean, *Deep Sea Res., Part I*, *48*, 1905–1921.

Weiss, R. F., and B. A. Price (1980), Nitrous oxide solubility in water and seawater, *Mar. Chem.*, *8*, 347–359.

Westley, M. B., H. Yamagishi, B. N. Popp, and N. Yoshida (2006), Nitrous oxide cycling in the Black Sea inferred from stable isotope and isotopomer distributions, *Deep Sea Res., Part II*, *53*(17–19), 1802–1816.

Westley, M. B., B. N. Popp, and T. M. Rust (2007), The calibration of the intramolecular nitrogen isotope distribution in nitrous oxide measured by isotope ratio mass spectrometry, *Rapid Commun. Mass Spectrom.*, *21*(3), 391–405.

Wrage, N., J. W. Van Groenigen, O. Oenema, and E. M. Baggs (2005), A novel dual-isotope labelling method for distinguishing between soil sources of N_2O, *Rapid Commun. Mass Spectrom.*, *19*(22), 3298–3306.

Yamagishi, H., N. Yoshida, S. Toyoda, B. N. Popp, M. B. Westley, and S. Watanabe (2005), Contributions of denitrification and mixing on the distribution of nitrous oxide in the North Pacific, *Geophys. Res. Lett.*, *32*, L04603, doi:10.1029/2004GL021458.

Yamagishi, H., M. B. Westley, B. N. Popp, S. Toyoda, N. Yoshida, S. Watanabe, K. Koba, and Y. Yamanaka (2007), Role of nitrification and denitrification on the nitrous oxide cycle in the eastern tropical North Pacific and Gulf of California, *J. Geophys. Res.*, *112*, G02015, doi:10.1029/2006JG000227.

Yoshida, N., and S. Toyoda (2000), Constraining the atmospheric N_2O budget from intramolecular site preference in N_2O isotopomers, *Nature*, *405*, 330–334.

Yoshida, N., H. Morimoto, M. Hirano, I. Koike, S. Matsuo, E. Wada, T. Saino, and A. Hattori (1989), Nitrification rates and ^{15}N abundances of N_2O and NO_3^- in the western North Pacific, *Nature*, *342*, 895–897.

Yoshinari, T. (1976), Nitrous oxide in the Sea, *Mar. Chem.*, *4*, 189–202.

Zamora, L. M., A. Oschlies, H. W. Bange, K. B. Huebert, J. D. Craig, A. Kock, and C. R. Löscher (2012), Nitrous oxide dynamics in low oxygen regions of the Pacific: Insights from the MEMENTO database, *Biogeosciences*, *9*(12), 5007–5022.